PREVIEWMAGAZINE

ISSUE THREE ▪ WWW.SNMMI.ORG/VIRTUALPREVIEW2

SNMMI Value Initiative
SOCIETY OF NUCLEAR MEDICINE & MOLECULAR IMAGING

July 11-14

SNMMI2020 ANNUAL MEETING

VIRTUAL Edition

Diagnosis to Therapy The Future of Image-Guided Patient Management

In This Issue

▶ **And The Winners Are...**
View this year's list of award winners!

▶ **Virtual Networking**
Receptions, Drink & Thinks, Movie Night, and more!

Expected results. **Delivered.**

Are you getting the most out of your Rb-82 Generator?

The RUBY-FILL® Rubidium 82 Generator is clinically proven to deliver industry-leading efficiency with reliable consistency and dosing flexibility[1-3]

RUBY-FILL® has been proven to

Consistently deliver expected yield with nearly 100% accuracy

- In a recent study comparing currently available generators, RUBY-FILL® showed industry-leading efficiency[3]

Deliver highly accurate patient doses

- Over the life of the generator, the deviation of delivered dose vs. requested dose approached 0%[3]

Provide clinical flexibility

- RUBY-FILL® provides a long shelf life and flexible, patient-specific dosing[1]

Seem unbelievable?
Visit **Jubilant Radiopharma** at the SNMMI Virtual Meeting Online July 11- 13 to see for yourself

RUBY FILL®
RUBIDIUM Rb82 GENERATOR

Indication for Use: RUBY-FILL is a closed system used to produce rubidium (Rb-82) chloride injection for intravenous use. Rubidium (Rb-82) chloride injection is a radioactive diagnostic agent indicated for Positron Emission Tomography (PET) imaging of the myocardium under rest or pharmacologic stress conditions to evaluate regional myocardial perfusion in adult patients with suspected or existing coronary artery disease.

New Important Safety Information April 2019
Please note changes in Boxed Warning, Dosage and Administration, Directions for Eluting Rubidium Rb 82 Chloride Injection (2.5), Contraindications (4), Warnings and Precautions, High Level Radiation Exposure with Use of Incorrect Eluent (5.1).

WARNING: HIGH LEVEL RADIATION EXPOSURE WITH USE OF INCORRECT ELUENT AND FAILURE TO FOLLOW QUALITY CONTROL TESTING PROCEDURE

Please see full prescribing information for complete boxed warning

High Level Radiation Exposure with Use of Incorrect Eluent
Using the incorrect eluent can cause high Strontium (Sr 82) and (Sr 85) breakthrough levels (5.1)

- Use only additive-free 0.9% Sodium Chloride Injection USP to elute the generator (2.5)
- Immediately stop the patient infusion and discontinue the use of the affected RUBY-FILL generator if the incorrect solution is used to elute the generator (4)
- Evaluate the patient's radiation absorbed dose and monitor for the effects of radiation to critical organs such as bone marrow (2.9)

Excess Radiation Exposure with Failure to Follow Quality Control Testing Procedure
Excess radiation exposure occurs when the levels of Sr 82 or Sr 85 in the rubidium Rb 82 chloride injection exceed specified limits (5.2)

- Strictly adhere to the generator quality control testing procedure (2.6)
- Stop use of a generator at any of its Expiration Limits (2.7)

The risk information provided here is not comprehensive. Please visit RUBY-FILL.com for full Prescribing Information including BOXED WARNING.

You are encouraged to report negative side effects of prescription drugs to the FDA. Visit www.fda.gov/Safety/MedWatch or call 1-800-FDA-1088.

References: 1. RUBY-FILL [package insert]. Kirkland, Quebec, Canada: Jubilant DraxImage Inc; April 2019. **2.** Renaud JM, Wiles M, Garrard L, Beanlands RSB, deKemp RA. New rubidium-82 generator efficiency improves over time. *J Nucl Med.* 2018;59(suppl 1):1045. **3.** Lewin HC, Millard A. Dose accuracy of 82Rb generator systems. Paper presented at: SNMMI Mid-Winter Meeting; January 17–19, 2019; Palm Springs, CA.

JUBILANT RADIOPHARMA

RUBY-FILL® is a registered trademark used under license by Jubilant DraxImage, Inc.
Jubilant DraxImage Inc. dba Jubilant Radiopharma, 16751 Trans-Canada Highway, Kirkland, Quebec, Canada H9H 4J4
Phone: 1.888.633.5343 / 514.630. 7080 Fax: 1.866.431.4288 / 514.694.3865 www.jubilantradiopharma.com
© Jubilant DraxImage Inc. 2019-US-RUBY-00018

A Re-Imagined Experience: Virtually Connecting You with Your Colleagues from Around the World!

The **SNMMI 2020 Annual Meeting - Virtual Edition**—Saturday, July 11 through Tuesday, July 14—gives you the unique opportunity to attend live continuing education sessions, review hundreds of scientific abstracts, connect with suppliers in the exhibit hall, and network with other attendees—**all in an exciting, interactive virtual environment**.

Best of all, the easy-to-use platform will mimic the dynamics of an in-person event, making it easy to navigate around and take full advantage of all the features the meeting has to offer. All you will need is an internet connection!

The SNMMI Annual Meeting - Virtual Edition connects you with:

An Immersive Virtual Learning Experience

More than 25 one-hour sessions will be available over 3.5 days, featuring live chat functionality during live broadcasts of the presentations. Miss a session? Each session will be available for on-demand viewing following its live broadcast.

Leading Research in the New Science Pavilion

View abstract presentations and posters of the profession's latest research, including recorded oral presentations from the authors. You will also be able to ask the authors questions by emailing them while visiting their poster/abstract.

Industry Suppliers in an Interactive Exhibit Hall

Visit customized virtual booths from top suppliers and learn more about their products/services through videos and downloadable presentations. Plus, connect through one-on-one meetings with exhibit personnel while visiting their booth.

Innovative Networking Opportunities

Interact with fellow attendees through one-on-one and group chat, and during great networking events, including Molecular Hub Meet-Ups, Saturday night Movie Viewing Party, the Presidents' Town Hall and Reception, and more.

No Registration Fee for SNMMI Members

Although registration is required, the Annual Meeting - Virtual Edition is free for SNMMI members. Non-members may either join SNMMI to attend at no cost or pay a modest fee. ***Please note: registration closes at 11:59 pm ET on Thursday, July 9.***

WWW.SNMMI.ORG/VIRTUALPREVIEW

THANK YOU TO OUR TITLE SPONSOR

We would like to recognize our title sponsor, Advanced Accelerator Applications, a Novartis Company, for their generous support of the SNMMI 2020 Annual Meeting - Virtual Edition.

Advanced Accelerator Applications
A Novartis Company

Earn up to 24 continuing education credits.

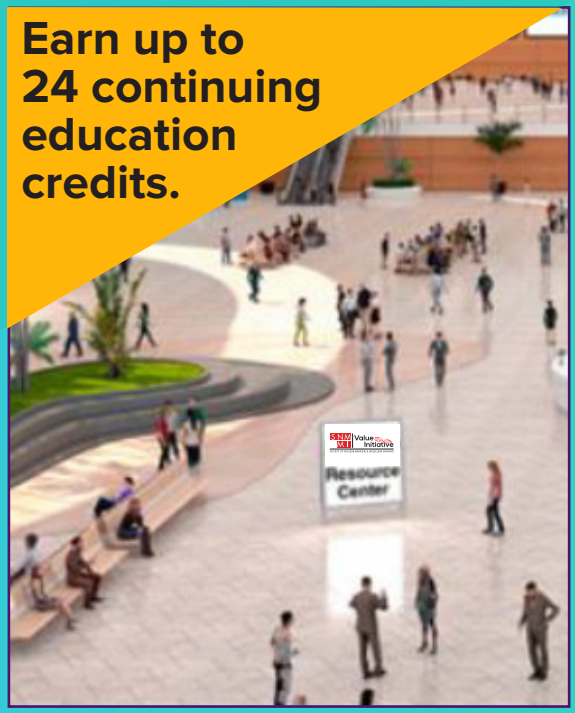

SNMMI WOULD LIKE TO RECOGNIZE & CONGRATULATE ITS 2020 AWARD WINNERS

2020 Paul C. Aebersold Award

The Aebersold Award is named for Paul C. Aebersold—a pioneer in the biologic and medical application of radioactive materials and the first director of the Atomic Energy Commission's Division of Isotope Development. It recognizes outstanding achievement in basic science applied to nuclear medicine and was first presented in 1973. *This prestigious award is presented annually at the SNMMI Annual Meeting and will be announced during the plenary session on Monday, July 13.*

2020 Georg Charles de Hevesy Award

Each year, SNMMI presents the Georg Charles de Hevesy Nuclear Medicine Pioneer Award to an individual for outstanding contributions to the field of nuclear medicine. De Hevesy received the 1943 Nobel Prize in chemistry for his work in determining the absorption, distribution, metabolism, and elimination of radioactive compounds in the human body. His work led to the foundation of nuclear medicine as a tool for diagnosis and therapy, and he is considered to be one of the fathers of nuclear medicine. *The winner of this year's award will be announced during the plenary session on Sunday, July 12.*

2020 Benedict Cassen Prize for Research in Molecular Imaging

The Cassen Prize and lecture honors Benedict Cassen, whose invention of the rectilinear radioisotope scanner—the first instrument capable of making an image of radiotracer distribution in body organs of living patients—was seminal to the development of clinical nuclear medicine. This award, given every other year, is funded through the Education and Research Foundation. *This year's recipient will be announced and give a lecture during the plenary session on Monday, July 13.*

2020 AWARD WINNERS

The **2020 SNMMI Presidential Distinguished Service Award** is given to individuals who made a significant impact within SNMMI over the past year. The individuals being recognized this year have shown exceptional leadership and have provided strategic guidance as the SNMMI navigated through this unprecedented time.

Wengen Chen, MD, PhD

Johannes Czernin, MD

Sharon Gleason

Nancy Knight, PhD

Sijin Li, MD, PhD

Rebecca Maxey

Vince Pistilli

Hongcheng Shi, MD, PhD

The **2020 SNMMI Presidential Distinguished Educator Awards** recognize SNMMI members who have demonstrated outstanding service and dedication to the field of nuclear medicine through their educational efforts.

Thomas H. Schindler, MD

Katherine Zukotynski, BASc, MD, FRCPC

The **2020 SNMMI-TS Presidential Distinguished Service Award** is given to individuals who made a significant impact within the SNMMI-TS over the last year. The individuals being recognized this year have shown exceptional leadership and have provided strategic guidance as the SNMMI-TS navigated through this unprecedented time.

Norman E. Bolus, MSPH, MPH, CNMT, FSNMMI-TS

Kathleen M. Krisak, BS, CNMT, FSNMMI-TS

Jennifer Prekeges, MS, CNMT

Anita M.Slechta MS, BSRT, RT(R)(M), FASRT, REHS

Anthony J. Sicignano, BS, CNMT, RT(N), FSNMMI-TS

SIEMENS Healthineers

James Williams, PhD; Karin Karl; and Ernest "Rocky" Humphreys

Paula McLean, CNMT; Kevin Boyle; Kieran Murphy; and Nathan Hermony

2020 AWARD WINNERS

The **SNMMI-TS/ERF Outstanding Educator Award** recognizes SNMMI-TS members who have demonstrated outstanding service and dedication to the field of nuclear medicine technology.

Geoffrey M. Currie, Bpharm, MMedRadSc, MAppMngt, MBA, PhD, AM

The **SNMMI-TS/ERF Outstanding Technologist Award** recognizes SNMMI-TS members who have demonstrated outstanding service and dedication to the field of nuclear medicine technology.

Matthew C. McMahon, MS, CNMT, RT(CT)

The **SNMMI-TS Advocate-of-the-Year** is awarded to an individual who has made significant contributions to advancing advocacy efforts at the state and federal level.

Lynne T. Roy, MBA, CNMT, FSNMMI-TS

Henry N. Wagner, Jr., MD Lectureship
Jagat Narula, MD, PhD, MACC

Berson-Yalow Award
Reinier Hernandez, PhD

Ursula Mary Kocemba-Slosky, PhD Professional Relations Fellowship
Lucas Gross, CNMT

Robert E. Henkin, MD, Government Relations Fellowship
Justin Peacock, MD, PhD
Domnique Newallo, MD

Mitzi & William Blahd, MD, Pilot Research Grant
Mark Dornan, PhD

ERF SNMMI CMIIT Laboratory Professional Recognition Award for Contributions to Molecular Imaging
Catherine Hou

Bradley-Alavi Student Fellowships
Matthew Dilsizian
Yangson Zhu
Zachary Rosenkrans

Wagner-Torizuka Fellowship Program
Funded by (Nihon Medhi-Physics)
Dr. Masatoshi Hott
Dr. Keiichiro Kuronuma
Dr. Yuichi Wakabayashi

PDEF Mickey Williams Minority Scholarship
Louise Nathalie Ngalle Moukoulou
Vanessa Ducharme

PDEF Professional Development Scholarship
Jay Smith

Susan C. Weiss Clinical Advancement Scholarship
Sarah Gibbons
Jamie Warren
Nickie Beaulieu

ERF SNMMI-TS Bachelor's or Master's Degree Completion Scholarship
Sarah Gibbons
Jordon Jayne

ERF SNMMI-TS Advanced Degree Scholarship
Mary Beth Farrell

Paul Cole Technologist Scholarship
Rafat Mohamed
Kye Broom
Jean Pierre Alfonso
Amanda Lima
Alannah Macaulay
Desiree Dinko
Alexandra Herman
Jordan Gottsacker
Sheryl Dekker
Mckenzie Wills

2020 NAMED AWARD LECTURESHIPS

BARRY SIEGEL LECTURESHIP AWARD

Sponsored by the Correlative Imaging Council

Richard Wahl, MD

"PERCISTence," PET/CT for Quantitative Assessment of Treatment Response

The Correlative Imaging Council Barry Siegel Lecture award will honor an individual who had made groundbreaking and consistent educational contributions to correlative imaging and to SNMMI and CIC. Dr. Barry Siegel made outstanding contributions to correlative imaging, namely, regarding the National Oncologic PET Registry (NOPR) and its tremendous impact on PET/CT imaging and reimbursement.

EDWARD J. HOFFMAN MEMORIAL AWARD LECTURE

Sponsored by the Physics, Instrumentation and Data Sciences Council

Dimitris Visvikis, PhD

"Quantitative multimodality imaging in the era of big data science"

The highest award of SNMMI's Computer and Instrumentation Council was created to honor the memory of Professor Edward J. Hoffman. It recognizes scientists in the field of nuclear medicine for their service and devotion to research and development of nuclear medicine instrumentation and to educating and training the next generation of scientists.

MICHAEL J. WELCH, PhD AWARD LECTURE

Sponsored by the Radiopharmaceutical Sciences Council

Henry VanBrocklin, PhD

"Life is Like a Box of Chocolates: A Molecular Imaging Journey"

The Michael J. Welch, PhD Award recognizes individuals who have made an outstanding contribution to the field of radiopharmaceutical sciences, have been involved in mentoring students, postdoctoral fellows and junior faculty, and have been involved in community service to the field of radiopharmaceutical chemistry and molecular imaging. Funded through an endowed gift given to the Education and Research Foundation for Nuclear Medicine and Molecular Imaging (ERF) by the Dr. Michael J. Welch Foundation.

GCNMC LECTURESHIP AWARD

Sponsored by the General Clinical Nuclear Medicine Council

Herbert Chen, MD, FACS

"Radioguided Techniques during Parathyroid Surgery"

The GCNMC Lectureship recognizes a speaker who will present insights on the value of general clinical nuclear medicine in clinical practice as procedures, which remain bread-&-butter studies in many departments, paved the way for today's targeted imaging and therapy and many of today's nuclear medicine practitioners owe their careers to these procedures.

2020 NAMED AWARD LECTURESHIPS

HERMANN BLUMGART AWARD LECTURE

Sponsored by the Cardiovascular Council

Piotr Slomka, PhD, FACC, FCCPM

"A Celebration of Excellence"

The Hermann Blumgart Award is the highest award and honor bestowed by the Cardiovascular Council, based on scientific contributions to the field of cardiovascular nuclear medicine and service to the Council.

OUTSTANDING EDUCATOR AWARD and LECTURESHIP

Sponsored by the Cardiovascular Council

Awarded to Diwakar Jain MD, FACC, FRCP, FASNC

The Outstanding Educator Award and Lectureship recognizes a current CVC member who has made extraordinary and consistent educational contributions to the nuclear cardiology community and to the SNMMI

KUHL-LASSEN AWARD LECTURE

Sponsored by the Brain Imaging Council

Nicolaas Bohnen, MD, PhD

"TI: Cholinergic imaging: new insights from multimodal approaches"

The highest award of SNMMI's Brain Imaging Council was created to honor two founding pioneers in functional brain imaging: SNMMI member David E. Kuhl, M.D., and Nils Lassen. The Kuhl-Lassen Award is given annually to recognize a scientist who has made outstanding contributions and whose research in and service to the discipline of functional brain imaging is of the highest caliber.

LOEVINGER-BERMAN AWARD LECTURE

Sponsored by the Medical Internal Radiation Dose (MIRD) Committee

Marta Cremonesi, PhD

"Calculation of patient-specific absorbed doses: Is it achievable – and practical?"

The award is given in recognition of excellence pertaining to the field of internal dosimetry as it relates to nuclear medicine through: research and/or development, significant publication contributions, or advancement of the understanding of internal dosimetry in relationship to risk and therapeutic efficacy.

PETER VALK MEMORIAL LECTURE

Sponsored by the PET Center of Excellence

Simon Cherry, PhD and Ramsey Badawi, PhD

"Total-Body PET with EXPLORER: Past, Present and Future"

The Peter E. Valk, MD Memorial Lectureship and Award was created to honor the memory of Dr. Valk, a pioneer in the establishment of PET as an important clinical study. This Award recognizes individuals who have made significant contributions to the advancement of PET, including PET/CT, PET/MRI and other emerging technologies, as well as those individuals who are dedicated to the PET Center of Excellence.

2020 SNMMI COUNCIL AWARDS

SAUL HERTZ AWARD SYMPOSIUM

Sponsored by the Therapy Center of Excellence

Douglas Van Nostrand, MD

"Frontiers of I-131 Therapy in Differentiated Thyroid Cancer"

SNMMI has established The Dr. Saul Hertz Lifetime Achievement Award in honor of the professional achievements of Dr. Hertz as the pioneer of Radioiodine Therapy. The award recognizes individuals who have made outstanding contributions to radionuclide therapy.

GCNMC LIFETIME ACHIEVEMENT AWARD

Sponsored by the General Clinical Nuclear Medicine Council

Awarded to Ora Israel, Sr., MD, FSNMMI

The GCNMC Lifetime Achievement Award is established to recognize those physicians and scientists who have distinguished themselves through a career dedicated to the advancement of patient care through the field of Nuclear Medicine. These individuals will have provided outstanding contributions to the general nuclear medicine subspecialties including urogenital, pulmonary, musculoskeletal, endocrine and gastrointestinal imaging that have advanced the field to allow improved clinical diagnosis and patient care.

MICHAEL J. WELCH POST-DOCTORAL TRAVEL GRANT

Sponsored by the Radiopharmaceutical Sciences Council

Awarded to Zhen Yang, PhD

The Michael J. Welch Post-Doctoral Travel Grant is given to a post-doctoral individual who has demonstrated a novel approach to radiochemistry. The Travel Grant is funded through an endowed gift given to the Education and Research Foundation for Nuclear Medicine and Molecular Imaging (ERF) by the Dr. Michael J. Welch Foundation.

TRACY LYNNE FABER MEMORIAL AWARD

Sponsored by the Physics, Instrumentation and Data Sciences Council

Awarded to Fanny Orlhac, PhD

The Tracy Lynn Faber Memorial Award is given each year to support advancement of women in medical imaging sciences. The Award is given either to an individual who has significantly promoted the advancement of women in medical imaging sciences, or to a woman in early- or mid-career who has made honor more significant contributions to medical imaging sciences. The endowment for the Tracy Lynn Faber Memorial Award is maintained by Emory University, Atlanta, GA.

2020 ALAVI–MANDELL AWARDS
FOR JNM ARTICLES PUBLISHED IN 2019

Parameters to Predict Progression Free and Overall Survival After Peptide Receptor Radionuclide Therapy: A Multivariate Analysis in 782 Patients
Else Aalbersberg

^{18}F-Fluciclovine Parameters on Targeted Prostate Biopsy Associated With True Positivity in Recurrent Prostate Cancer
Olayinka Abiodun-Ojo

Frequency, Determinants, and Costs of Recommendations for Additional Imaging in Clinical FDG-PET/CT Reports
Hasan Alesawi

Assessment of Physiological Intracranial Calcification in Healthy Adults Using ^{18}F-NaF PET/CT
Abdullah Al-Zaghal

rA1M is a Potential Kidney Protector in ^{177}Lu-Octreotate Treatment of Neuroendocrine Tumors
Charlotte Andersson

Does Measurement of ^{18}F-fluoride Metabolic Flux Improve Response Assessment of Breast Cancer Bone Metastases Compared With Standardised Uptake Values in ^{18}F-Fluoride PET/CT?
Gurdip Azad

Thyroid Uptake and Effective Half-Life of Radioiodine in Thyroid Cancer Patients at Radioiodine Therapy and Follow-up Whole-Body Scintigraphy Either in Hypothyroidism or Under rhTSH
Robin Bacher

The Characterization of ^{18}F-hGTS13 for Molecular Imaging of xC- Transporter Activity With Positron Emission Tomography
Corinne Beinat

^{18}F-FDG-PET/CT-Guided Treatment Duration in Patients With High-Risk Staphylococcus Aureus Bacteremia: A Proof of Principle
Marvin Berrevoets

Deep Learning Analysis of Upright-Supine High-Efficiency SPECT Myocardial Perfusion Imaging for Prediction of Obstructive Coronary Artery Disease: A Multicenter Study
Julian Betancur

In Vivo Characterization and Quantification of Neurofibrillary Tau PET Radioligand [^{18}F]MK-6240 in Humans from Alzheimer's Disease Dementia to Young Controls
Tobey Betthauser

Detection at Public Facilities of ^{131}I in Patients Treated for Differentiated Thyroid Cancer: The Frequency, Sites, Management by Security Agents, and Recommended Physician Documentation for Patients
Athanasios Bikas

Principal Component Analysis of Brain Metabolism Predicts Development of Alzheimer's Dementia
Ganna Blazhenets

Diastereomerically Pure 6*R*- and 6*S*-3′-aza-2′;^{18}F-Fluoro-5-Methyltetrahydrofolates Show Unprecedented High Uptake in Folate Receptor-positive KB Tumors
Silvan Boss

Affibody-Based PET Imaging to Guide EGFR-Targeted Cancer Therapy in Head and Neck Squamous Cell Cancer Models
Thomas Burley

Prognostic Value of SUR in Patients With Trimodality Treatment of Locally Advanced Esophageal Carcinoma
Rebecca Bütof

PARaDIM–A PHITS-based Monte Carlo tool for internal dosimetry with tetrahedral mesh computational phantoms
Lukas Carter

^{11}C-DPA-713 versus ^{18}F-GE-180: A preclinical comparison of TSPO-PET tracers to visualize acute and chronic neuroinflammation in a mouse model of ischemic stroke
Aisling Chaney

An Efficient Approach to Perform MR-assisted PET Data Optimization in Simultaneous PET/MR Neuroimaging Studies
Kevin Chen

Combination of ^{68}Ga-PSMA PET/CT and multiparameter MRI improves the detection of clinically significant prostate cancer: a lesion by lesion analysis
Mengxia Chen

Assessing Amyloid Pathology in Cognitively Normal Subjects using [^{18}F]Flutemetamol PET: Comparing Visual Reads and Quantitative Methods
Lyduine Collij

^{18}F-HX4 Hypoxia PET Holds Promise as a Prognostic and Predictive Imaging Biomarker in a Lung Cancer Xenograft Model Treated with Metformin and Radiotherapy
Sven De Bruycker

2020 ALAVI–MANDELL AWARDS
FOR JNM ARTICLES PUBLISHED IN 2019

Galectin-3 Targeting in Thyroid Orthotopic Tumors Opens New Ways to Characterize Thyroid Cancer
Francesco De Rose

Immuno-PET of Innate Immune Markers CD11b and IL-β Detect Inflammation in Murine Colitis
Nicole Dmochowska

The Relationship Between Tumour Glucose Metabolism and Host Systemic Inflammatory Responses in Patients With Cancer: A Systematic Review
Ross Dolan

MEK Inhibition Induces Therapeutic Iodine Uptake in a Murine Model of Anaplastic Thyroid Cancer
Oussama ElMokh

Early and Longitudinal Microglial Activation but not Amyloid Accumulation Predict Cognitive Outcome in PS2APP Mice
Carola Focke

Measurement Repeatability of ^{18}F-FDG-PET/CT Versus ^{18}F-FDG-PET/MRI in Solid Tumors of the Pelvis
Tyler Fraum

P2X7 Radioligand ^{18}F-PTTP for the Differentiation of Lung Tumor and Inflammation
Zhequan Fu

Early Experience of Rechallenge ^{177}Lu-PSMA Radioligand Therapy After an Initial Good Response in Patients With mCRPC
Andrei Gafita

qPSMA: A Semi-Automatic Software for Whole-Body Tumor Burden Assessment in Prostate Cancer Using ^{68}Ga-PSMA11 PET/CT
Andrei Gafita

A Prospective Observational Study to Evaluate the Effects of Long-Acting Somatostatin Analogs on ^{68}Ga-DOTATATE Uptake in Patients With Neuroendocrine Tumors
Anni Gålne

Identification and Preclinical Evaluation of a Radiofluorinated Benzazepine Derivative for Imaging the GluN2B Subunit of the Ionotropic NMDA Receptor
Ahmed Haider

Preclinical Evaluation of Benzazepine-Based PET Radioligands (R)- and (S)-^{11}C-Me-NB1 Reveals Distinct Enantiomeric Binding Patterns and Tightrope Walk between GluN2B- and Sigma1 Receptor-Targeted PET Imaging
Ahmed Haider

Preclinical Evaluation of ^{111}In-labeled PEGylated Maytansine Nimotuzumab Drug Conjugates in EGFR-positive Cancer Models
Siddesh Hartimath

^{177}Lu-NM600 Targeted Radionuclide Therapy Extends Survival in Syngeneic Murine Models of Triple-Negative Breast Cancer
Reinier Hernandez

Tumor Lysis Syndrome: A Rare, but Serious Complication of Radioligand Therapies
Kai Huang

Generation of PET Attenuation Map for Whole-Body Time-of-Flight ^{18}F-FDG PET/MRI Using a Deep Neural Network Trained With Simultaneously Reconstructed Activity and Attenuation Maps
Donghwi Hwang

F-18 FDG PET/CT for Monitoring of Ipilimumab Therapy in Patients With Metastatic Melanoma
Kimiteru Ito

Healthy Tissue Uptake of ^{68}Ga-Prostate Specific Membrane Antigen (PSMA), ^{18}F-DCFPyL, ^{18}F-Fluoromethylcholine (FCH) and ^{18}F-Dihydrotestosterone (FDHT)
Bernard Jansen

Simplified Methods for Quantification of ^{18}F-DCFPyL Uptake in Patients with Prostate Cancer
Bernard Jansen

^{89}Zr-immuno-PET: Towards a Non-Invasive Clinical Tool to Measure Target Engagement of Therapeutic Antibodies In-vivo
Yvonne Jauw

Quantitative Tumor Perfusion Imaging With ^{82}Rubidium-PET/CT in Prostate Cancer – Analytical and Clinical Validation
Mads Jochumsen

Design of Cerenkov-assisted Photoactivation of TiO_2 Nanoparticles and Reactive Oxygen Species Generation for Cancer Treatment
Shalinee Kavadiya

Albumin-Binding PSMA Ligands: Implications for Expanding the Therapeutic Window
James Kelly

Blocking Glucagon Like Peptide-1 Receptors in the Exocrine Pancreas Improves Specificity for Beta Cells in a Mouse Model of Type 1 Diabetes
Eshita Khera

2020 ALAVI–MANDELL AWARDS
FOR JNM ARTICLES PUBLISHED IN 2019

DOTA-MGS5, a New Cholecystokinin-2 Receptor Targeting Peptide Analog With Optimized Targeting Profile for Theranostic Use
Maximilian Klingler

Assessment of Simplified Methods for Quantification of ^{18}F-FDHT Uptake in Patients With Metastatic Castration-Resistant Prostate Cancer
Gerbrand Kramer

^{18}F-Fluoroestradiol Positron Emission Tomography Imaging of Activating Estrogen Receptor Alpha Mutations in Breast Cancer
Manoj Kumar

One-step ^{18}F-Labeling and Preclinical Evaluation of Prostate Specific Membrane Antigen Trifluoroborate Probes for Cancer Imaging
Hsiou-Ting Kuo

Three-hour Delayed Imaging Improves Assessment of Coronary ^{18}F-Sodium Fluoride PET
Jacek Kwiecinski

Data-driven Gross Patient Motion Detection and Compensation: Implications for Coronary ^{18}F-NaF PET Imaging
Martin Lyngby Lassen

Improving 68-Ga-PSMA PET/MR Hybrid Imaging of the Prostate With Un-renormalized Absolute Scatter Correction
Maike Lindemann

Preclinical Evaluation and Pilot Clinical Study of Al ^{18}F-PSMA-BCH for Prostate Cancer Imaging
Teli Liu

^{68}Ga-pentixafor PET/CT for imaging of chemokine receptor-4 expression in Waldenström macroglobulinemia/lymphoplasmacytic lymphoma: comparison to ^{18}F-FDG PET/CT
Yaping Luo

In vitro and in vivo characterization of a ^{18}F-AlF-labeled PSMA ligand for imaging of PSMA-expressing xenografts
Susanne Lütje

Preclinical pharmacokinetics and dosimetry studies of [^{124}I/^{131}I]-CLR1404 for treatment of pediatric solid tumors in murine xenograft models
Ian Marsh

Side effects of CXC-chemokine receptor 4 – directed Endoradiotherapy with Pentixather prior to Hematopoietic Stem Cell Transplantation
Sabine Maurer

Imaging chemotherapy induced acute cardiotoxicity with ^{18}F-labelled lipophilic cations
Stuart McCluskey

Three dimensional tumor-margin demarcation using the hybrid tracer indocyanine green-^{99m}Tc-nanocolloid, a proof of concept study in tongue cancer patients scheduled for sentinel node biopsy
Philippa Meershoek

Evaluation of a Novel Elastic Respiratory Motion Correction Algorithm on Quantification and Image Quality in Abdomino-thoracic PET/CT
Joseph Meier

Metabolic Tumour Volume for Response Prediction in Advanced-Stage Hodgkin Lymphoma
Jasmin Mettler

Awake ^{18}F-FDG PET Imaging of Memantine-Induced Brain Activation and Test-Retest in Freely Running Mice
Alan Miranda

Cerebral Metabolic Changes Related to Freezing of Gait in Parkinson's Disease
Trina Mitchell

^{18}F-Branched Chain Amino Acids: Structure-Activity Relationships and PET Imaging Potential
Matthew Nodwell

Optimized Feature Extraction for Radiomics Analysis of ^{18}F-FDG-PET Imaging
Laszlo Papp

Evaluation of a Novel PET Radioligand to Image O-GlcNAcase in Brain and Periphery of Rhesus Monkey and Knock-Out Mouse
Soumen Paul

Temporal Modulation of HER2 Membrane Availability Increases Pertuzumab Uptake and Pretargeted Molecular Imaging of Gastric Tumors
Patricia Pereira

Radiation Dosimetry and Biodistribution of ^{18}F-PSMA-11 for PET Imaging of Prostate Cancer
Sarah Piron

N-(2-(Dimethylamino)Ethyl)-4-18F-Fluorobenzamide: A Novel Molecular Probe for High-Contrast PET Imaging of Malignant Melanoma
Ayoung Pyo

Production of ^{15}O for Medical Applications Via the ^{16}O(Y,n) ^{15}O Reaction
Stacy Queern

2020 ALAVI–MANDELL AWARDS
FOR JNM ARTICLES PUBLISHED IN 2019

Dosimetry Estimate and Initial Clinical Experience With ^{90}Y-PSMA-617
Hendrik Rathke

PET/CT Versus Standard Imaging for Prediction of Survival in Patients with Recurrent Head and Neck Squamous Cell Carcinoma
Max Rohde

Multispectral Optoacoustic Tomography of Benign and Malignant Thyroid Disorders - A Pilot Study
Wolfgang Roll

Longitudinal PET Monitoring of Amyloidosis and Microglial Activation in a Second Generation Amyloid-beta Mouse Model
Christian Sacher

Sensitivity and Isoform Specificity of ^{18}F-Fluorofuranylnorprogesterone for Measuring Progesterone Receptor Protein Response to Estradiol Challenge in Breast Cancer
Kelley Salem

Impact of ^{68}Ga-PSMA-PET/CT on the Radiotherapeutic Approach for Prostate Cancer in Comparison to CT – A Retrospective Analysis
Nina-Sophie Schmidt-Hegemann

Outcome After PSMA PET/CT Based Salvage Radiotherapy in Patients with Biochemical Recurrence After Radical Prostatectomy: A Bi-institutional Retrospective Analysis
Nina-Sophie Schmidt-Hegemann

Quantitative Imaging Biomarkers for Yttrium-90 Distribution on Bremsstrahlung Single Photon Emission Computed Tomography After Resin-Based Radioembolization
Isabel Schobert

Dynamic ^{11}C-PiB PET Shows Cerebrospinal Fluid Flow Alterations in Alzheimer's Disease and Multiple Sclerosis
Julia Schubert

Intention to Treat Analysis of ^{68}Ga-PSMA and ^{11}C-choline PET/CT Versus CT for Prostate Cancer Recurrences After Surgery
Johannes Schwenck

Long-term Effects of Radioiodine Treatment on Salivary Gland Function in Adult Survivors of Pediatric Differentiated Thyroid Carcinoma
Tharsana Selvakumar

^{68}Ga-DOTA-E[c(RGDfK)]$_2$ Positron Emission Tomography Imaging of SHARPIN-Regulated Integrin Activity in Mice
Riikka Siitonen

Impact of ^{18}F-PSMA-1007 Uptake in Prostate Cancer Using Different Peptide Concentrations: Preclinical PET/CT Study in Mice
Fumihiko Soeda

Synthesis of Patient-Specific Transmission Image for PET Attenuation Correction for PET/MR Imaging of the Brain Using a Convolutional Neural Network’
Karl Spuhler

A Fully Automatic Technique For Precise Localization and Quantication of Amyloid-β; PET Scans
Mouna Tahmi

Dixon-VIBE Deep Learning (DIVIDE) Pseudo-CT Synthesis for Pelvis PET/MR Attenuation Correction
Angel Torrado-Carvajal

What FDG-PET Response-Assessment Method Best Predicts Survival After Curative-Intent Chemoradiation in Non-Small Cell Lung Cancer (NSCLC): EORTC, PERCIST, Peter Mac or Deauville Criteria?
Guy-Anne Turgeon

Accuracy of ^{18}F-FDG PET/CT in Predicting Residual Disease After Neoadjuvant Chemoradiotherapy for Esophageal Cancer
Maria Valkema

Metabolic Subtyping of Pheochromocytoma and Paraganglioma by ^{18}F-FDG Pharmacokinetics Using Dynamic PET/CT Scanning
Anouk van Berkel

A Pilot Study on Hepatobiliary Scintigraphy to Monitor Regional Liver Function in Yttrium-90 Radioembolization
Sandra van der Velden

The Clinical Application of Fluorescence-Guided Surgery in Head and Neck Cancer
Stan van Keulen

Performance Characteristics of the Digital Biograph Vision PET/CT System
Joyce van Sluis

Molecular Imaging of Fibroblast Activity After Myocardial Infarction Using a ^{68}Ga-labelled Fibroblast Activation Protein Inhibitor FAPI-04
Zohreh Varasteh

The Impact of FcγRI Binding on ImmunoPET
Delphine Vivier

Synergistic Effect of a Mesothelin Targeted Thorium-227 Conjugate in Combination with DNA Damage Response Inhibitors in Ovarian Cancer Xenograft Models
Katrine Wickstrøm

2020 ALAVI–MANDELL AWARDS
FOR JNM ARTICLES PUBLISHED IN 2019

PET Imaging of PARP Expression Using [^{18}F]Olaparib
Thomas Wilson

Tumor Imaging Using Radiolabelled Matrix Metalloproteinase-Activated Anthrax Proteins
Mary-Ann Xavier

Hexokinase 2 is Targetable for HK1 Negative, HK2 Positive Tumors From a Wide Variety of Tissues of Origin
Shili Xu

Biodistribution, Tumor Detection and Radiation Dosimetry of F-18 5-Fluoro-2′-Deoxycytidine (^{18}F-FdCyd) With Tetrahydrouridine in Solid Tumors
Colin Young

Advancing Targeted Radionuclide Therapy through the National Cancer Institute's Small Business Innovation Research Pathway
Kaveh Zakeri

Peptide Receptor Radionuclide Therapy in Grade 3 Neuroendocrine Neoplasms: Safety and Survival Analysis in 69 Patients
Jingjing Zhang

^{177}Lu-PSMA-617 Radioligand Therapy in Metastatic Castration-Resistant Prostate Cancer Patients With a Single Functioning Kidney
Jingjing Zhang

Variability and Repeatability of Quantitative Uptake Metrics in [^{18}F]FDG PET/CT Imaging of Non-small Cell Lung Cancer: Impact of Segmentation Method, Uptake Interval, and Reconstruction Protocol
Mingzan Zhuang

2020 INTERNATIONAL BEST ABSTRACT

- **Diego Passadore** — Argentina
- **Christopher Rowe** — Australia
- **Oana Kulterer** — Austria
- **Jonatan Dewulf** — Belgium
- **Isabella Palazzon** — Brazil
- **Sonya Sergieva** — Bulgaria
- **Ur Metser** — Canada
- **Meiqi Wu** — China
- **Gonzalo Ucros** — Colombia
- **Mads Jochumsen** — Denmark
- **Ahmed Kandeel** — Egypt
- **Francoise Kraeber-Bodéré** — France
- **Isabel Rauscher** — Germany
- **Georgios Papadakis** — Greece
- **Attila Forgacs** — Hungary
- **Kavita Bansal**— India
- **Febby Hutomo** — Indonesia
- **Rachel Bar-Shalom** — Israel
- **Gayane Aghakhanyan** — Italy
- **Tomohisa Okada** — Japan
- **Samuel Gitau** — Kenya
- **Haewook Park** — Republic of Korea
- **Abdulredha Esmail** — Kuwait
- **Joel Vargas** — Mexico
- **Jakoba Eertink** — Netherlands
- **Johan Blakkisrud** — Norway
- **Jacek Kwiecinski** — Poland
- **Mehdi Djekidel** — Qatar
- **Pavel Gelezhe** — Russian Federation
- **Abdullah Alqarni** — Saudi Arabia
- **Jasna Mihailovic** — Serbia
- **Ismaheel Lawal** — South Africa
- **Antonio Maldonado** — Spain
- **Sara Rinne** — Sweden
- **Irene Burger** — Switzerland
- **Tsung-Ying Ho** — Taiwan
- **Tanyaluck Thientunyakit** — Thailand
- **Bengul Gunalp** — Turkey
- **Edward ONeill** — United Kingdom
- **Ebrahim Delpassand** — United States
- **Omar Alonso** — Uruguay
- **Galal Alobthani** — Yemen

THE JOURNAL OF NUCLEAR MEDICINE
BEST PAPERS

▶ EDITORS' CHOICE AWARD — FOR THE BEST CLINICAL ARTICLE IN 2019

is presented to

Clemens Kratochwil, Paul Flechsig, Thomas Lindner, Labidi Abderrahim, Annette Altmann, Walter Mier, Sebastian Adeberg, Hendrik Rathke, Manuel Röhrich, Hauke Winter, Peter K. Plinkert, Frederik Marme, Matthias Lang, Hans-Ulrich Kauczor, Dirk Jäger, Jürgen Debus, Uwe Haberkorn, and Frederik L. Giesel

Department of Nuclear Medicine, University Hospital Heidelberg, Heidelberg, Germany

for

^{68}Ga-FAPI PET/CT: Tracer Uptake in 28 Different Kinds of Cancer

J Nucl Med. 2019; 60:801–805

▶ EDITORS' CHOICE AWARD — FOR THE BEST BASIC SCIENCE ARTICLE IN 2019

is presented to

Carola Focke, Tanja Blume, Benedikt Zott, Yuan Shi, Maximilian Deussing, Finn Peters, Claudio Schmidt, Gernot Kleinberger, Simon Lindner, Franz-Josef Gildehaus, Leonie Beyer, Barbara von Ungern-Sternberg, Peter Bartenstein, Laurence Ozmen, Karlheinz Baumann, Mario M. Dorostkar, Christian Haass, Helmuth Adelsberger, Jochen Herms, Axel Rominger, and Matthias Brendel

Department of Nuclear Medicine, University Hospital of Munich, LMU Munich, Munich, Germany

for

Early and Longitudinal Microglial Activation but Not Amyloid Accumulation Predicts Cognitive Outcome in PS2APP Mice

J Nucl Med. 2019; 60:548–554

▶ EDITORS' CHOICE AWARD — FOR THE OVERALL BEST ARTICLE IN 2019

is presented to

Clemens Kratochwil, Paul Flechsig, Thomas Lindner, Labidi Abderrahim, Annette Altmann, Walter Mier, Sebastian Adeberg, Hendrik Rathke, Manuel Röhrich, Hauke Winter, Peter K. Plinkert, Frederik Marme, Matthias Lang, Hans-Ulrich Kauczor, Dirk Jäger, Jürgen Debus, Uwe Haberkorn, and Frederik L. Giesel

Department of Nuclear Medicine, University Hospital Heidelberg, Heidelberg, Germany

for

^{68}Ga-FAPI PET/CT: Tracer Uptake in 28 Different Kinds of Cancer

J Nucl Med. 2019; 60:801–805

These exceptional articles are included on the following pages.

Downloaded from jnm.snmjournals.org by on March 26, 2020. For personal use only.

The Journal of NUCLEAR MEDICINE

Early and Longitudinal Microglial Activation but Not Amyloid Accumulation Predicts Cognitive Outcome in PS2APP Mice

Carola Focke, Tanja Blume, Benedikt Zott, Yuan Shi, Maximilian Deussing, Finn Peters, Claudio Schmidt, Gernot Kleinberger, Simon Lindner, Franz-Josef Gildehaus, Leonie Beyer, Barbara von Ungern-Sternberg, Peter Bartenstein, Laurence Ozmen, Karlheinz Baumann, Mario M. Dorostkar, Christian Haass, Helmuth Adelsberger, Jochen Herms, Axel Rominger and Matthias Brendel

J Nucl Med. 2019;60:548-554.
Published online: September 27, 2018.
Doi: 10.2967/jnumed.118.217703

This article and updated information are available at:
http://jnm.snmjournals.org/content/60/4/548

Information about reproducing figures, tables, or other portions of this article can be found online at:
http://jnm.snmjournals.org/site/misc/permission.xhtml

Information about subscriptions to JNM can be found at:
http://jnm.snmjournals.org/site/subscriptions/online.xhtml

The Journal of Nuclear Medicine is published monthly.
SNMMI | Society of Nuclear Medicine and Molecular Imaging
1850 Samuel Morse Drive, Reston, VA 20190.
(Print ISSN: 0161-5505, Online ISSN: 2159-662X)

© Copyright 2019 SNMMI; all rights reserved.

SNMMI SOCIETY OF NUCLEAR MEDICINE AND MOLECULAR IMAGING

Downloaded from jnm.snmjournals.org by on March 26, 2020. For personal use only.

FEATURED ARTICLE OF THE MONTH

Early and Longitudinal Microglial Activation but Not Amyloid Accumulation Predicts Cognitive Outcome in PS2APP Mice

Carola Focke*[1], Tanja Blume*[1,2], Benedikt Zott*[3], Yuan Shi*[2,4], Maximilian Deussing[1], Finn Peters[4], Claudio Schmidt[1], Gernot Kleinberger[5,6], Simon Lindner[1], Franz-Josef Gildehaus[1], Leonie Beyer[1], Barbara von Ungern-Sternberg[1], Peter Bartenstein[1,5], Laurence Ozmen[7], Karlheinz Baumann[7], Mario M. Dorostkar[2,4], Christian Haass[4–6], Helmuth Adelsberger[3], Jochen Herms[2,4,5], Axel Rominger[1,5,8], and Matthias Brendel[1,5]

[1]*Department of Nuclear Medicine, University Hospital of Munich, LMU Munich, Munich, Germany;* [2]*Center for Neuropathology and Prion Research, Ludwig-Maximilians-University of Munich, Munich, Germany;* [3]*Institute of Neuroscience, Technical University of Munich, Munich, Germany;* [4]*DZNE–German Center for Neurodegenerative Diseases, Munich, Germany;* [5]*Munich Cluster for Systems Neurology, University of Munich, Munich, Germany;* [6]*Biomedical Center, Biochemistry, Ludwig-Maximilians-University of Munich, Munich, Germany;* [7]*Roche Pharma Research and Early Development, F. Hoffmann-La Roche Ltd., Basel, Switzerland; and* [8]*Department of Nuclear Medicine, Inselspital, University Hospital Bern, Bern, Switzerland*

Neuroinflammation may have beneficial or detrimental net effects on the cognitive outcome of Alzheimer disease (AD) patients. PET imaging with 18-kDa translocator protein (TSPO) enables longitudinal monitoring of microglial activation in vivo. **Methods:** We compiled serial PET measures of TSPO and amyloid with terminal cognitive assessment (water maze) in an AD transgenic mouse model (PS2APP) from 8 to 13 mo of age, followed by immunohistochemical analyses of microglia, amyloid, and synaptic density. **Results:** Better cognitive outcome and higher synaptic density in PS2APP mice was predicted by higher TSPO expression at 8 mo. The progression of TSPO activation to 13 mo also showed a moderate association with spared cognition, but amyloidosis did not correlate with the cognitive outcome, regardless of the time point. **Conclusion:** This first PET investigation with longitudinal TSPO and amyloid PET together with terminal cognitive testing in an AD mouse model indicates that continuing microglial response seems to impart preserved cognitive performance.

Key Words: amyloid PET; TSPO PET; synaptic density; neuroinflammation; water maze

J Nucl Med 2019; 60:548–554
DOI: 10.2967/jnumed.118.217703

Alzheimer disease (AD) is the most common cause of dementia and is placing an ever more onerous burden on health care because of its exponentially rising incidence with increasing age (*1*). Immunologically mediated neuroinflammation is one hallmark of the pathophysiologic process of AD (*2,3*). Current models view neuroinflammation as a double-edged sword, which can have protective or detrimental effects on brain pathology, function, and the cognitive outcome (*4,5*). Microglia, the resident phagocytes of the innate immune system in the central nervous system, continuously survey for pathogens or cellular debris, secrete factors for tissue repair, and contribute to the plasticity of neuronal circuits by supporting the maintenance and remodeling of synapses (*6*). Microglia in AD brain can recognize and phagocytose soluble and fibrillary β-amyloid (Aβ), resulting in an increased inflammatory reaction (*2*). Although this kind of acute inflammation response promotes cellular repair and restores brain integrity, chronic inflammation processes can contribute to neurodegeneration (*7*).

Various transgenic mouse models of AD recapitulate neuroinflammatory processes in conjunction with classic Aβ pathology (*8,9*), and translational studies of these models are facilitated by small-animal PET with radioligands for imaging of AD biomarkers (*10,11*). The 18-kD translocator protein (TSPO), which is highly expressed at the outer mitochondrial membrane of activated microglia, presents a valuable biomarker for autoradiographic studies of microglial activation (*12,13*) and likewise for examination by PET of neuroinflammation in the brain of AD patients or in AD mouse models (*14*).

PET investigation of AD patients indicated only a low correlation between cerebral amyloid burden and cognitive performance (*15*), and Aβ deposition precedes the onset of neuroinflammation in patients with mild cognitive impairment (*16*). We contend that the temporal sequences of Aβ deposition and microglial activation in relation to progression of cognitive impairment is best examined through molecular imaging studies of longitudinal design. We have established this principle in serial PET examinations of Aβ accumulation in PS2APP mice treated with an experimental γ-secretase inhibitor (*17*).

Given this background, we aimed to correlate serial measures of TSPO and Aβ PET with terminal cognitive assessment in the PS2APP amyloid mouse model. Our goals were to, first, assess possible correlations between fibrillar amyloidosis in young and aged PS2APP mice with the cognitive outcome; second, determine whether early microglial response at baseline has an impact on the terminal cognitive outcome; and third, determine whether ongoing microglial activation influences the terminal cognitive outcome.

Received Jul. 16, 2018; revision accepted Sep. 10, 2018.
For correspondence or reprints contact: Matthias Brendel, Department of Nuclear Medicine, LMU Munich, Marchioninistraße 15, 81377 Munich, Germany.
E-mail: matthias.brendel@med.uni-muenchen.de
*Contributed equally to this work.
Published online Sep. 27, 2018.
COPYRIGHT © 2019 by the Society of Nuclear Medicine and Molecular Imaging.

Downloaded from jnm.snmjournals.org by on March 26, 2020. For personal use only.

MATERIALS AND METHODS

Study Design

All experiments were performed in compliance with the National Guidelines for Animal Protection, Germany, with approval of the local animal care committee of the Government of Oberbayern (Regierung Oberbayern) and overseen by a veterinarian. The study was performed in a longitudinal design starting with dual-tracer PET (TSPO and Aβ) at 8 mo of age as the first time point. Additional TSPO PET was performed at 9.5, 11.5, and 13 mo of age, and a final Aβ PET examination was performed at 13 mo. After recovering from the last PET scan, the mice were transferred to the behavioral facility and allowed to rest for 1 wk before initiation of the water maze (WM) tests of spatial learning. One week after this behavioral test, the mice were deeply anesthetized before transcardial perfusion. After brain extraction, we processed the brains for immunohistochemical and biochemical analyses (randomized hemispheres). Figure 1 illustrates the study design.

Animal Models and Statistical Power Analysis

We used 7 female wild-type C57BL/6 (WT) and 10 PS2APP transgenic mice in this investigation (*18,19*). The required sample sizes were calculated for correlation analyses (transgenic) and group comparisons (transgenic vs. WT) using G*power (version 3.1.9.2), based on assumptions for a type I error with an α-value of 0.05 and a power of 0.8. Effect size estimations were based on previous investigations with the same model. One additional animal was included per genotype to account for possible dropouts.

PET Imaging

PET Acquisition, Reconstruction, and Postprocessing. All PET procedures followed an established standardized protocol for radiochemistry, acquisition, and postprocessing (*14,20*). In brief, ^{18}F-GE180 TSPO PET (11.2 ± 1.5 MBq) with an emission window of 60–90 min after injection was used to measure cerebral TSPO expression, and ^{18}F-florbetaben Aβ PET (10.8 ± 1.5 MBq) with an emission window of 30–60 min after injection was used for assessment of fibrillary cerebral amyloidosis. All analyses were performed by PMOD (version 3.5; PMOD Technologies). Normalization of images to SUV or SUV ratio images was performed by the previously validated myocardium correction method (*21*) for TSPO PET and by a white matter reference region for Aβ PET (*20*).

PET Image Analysis. SD images (z score) were generated for all PS2APP mice for all time points and for both tracers. Here we used age-matched WT images (n = 7 each) specifically to calculate maps of the average (AVG_{WT}) and SD (SD_{WT}) of the relative SUV ratio for each tracer. Calculation of individual PS2APP z score images was performed by the formula $(PS2APP - AVG_{WT})/SD_{WT}$. Voxelwise maps for the area under the curve (AUC) of tracer uptake differences were calculated for each individual animal by generation or summation of z score averages between imaging time points weighted for the respective time gap. The following equations were used:

$$\text{TSPO PET AUC} = 6 \bullet \frac{TP1 + TP2}{2} + 8 \bullet \frac{TP2 + TP3}{2} + 6 \bullet \frac{TP3 + TP4}{2} \quad \text{Eq. 1}$$

$$\text{Aβ PET AUC} = 20 \bullet \frac{TP1 + TP4}{2}, \quad \text{Eq. 2}$$

where TP-1 is 8 mo old, TP-2 is 9.5 mo old, TP-3 is 11.5 mo old, and TP-4 is 13 mo old. Voxelwise correlation analyses of z score and AUC maps with behavioral results were performed by statistical parametric mapping (SPM) using SPM5 routines (Wellcome Department of Cognitive Neurology) implemented in MATLAB (version 7.1; MathWorks Inc.). For volume-of-interest (VOI)–based analyses, we applied 2 predefined VOIs. The first VOI was a large forebrain VOI comprising mainly neocortical and hippocampal regions with the highest amyloidosis in PS2APP mice (92 mm^3). The second VOI comprised brain areas associated with spatial learning, including the hippocampal formation, piriform and entorhinal cortices as well as the amygdala (32 mm^3). Additionally, VOIs of peak clusters deriving from the SPM analysis were applied for extraction of individual regional z scores. Correlation analysis of VOI-based z score PET values with other modalities was performed by calculating the Pearson coefficient of correlation.

WM

Mice were subjected to a modified WM task as described previously (*22–24*), yielding escape latency and distance to the correct platform as readouts.

Mice had to distinguish between 2 visible platforms, one of which was weighted in a way that it would float when the mouse climbed on (correct choice), whereas the other would sink (wrong choice). The correct platform was always located at the same spot in the maze, whereas the wrong platform as well as the site from which the mice were released into the maze was varied in a pseudorandom fashion. Visual cues on the walls of the laboratory provided orientation. Trials were terminated if the mouse failed to reach one of the platforms within 30 s (error of omission). In this case, or in case of a wrong choice, the experimenter placed the mouse on the correct platform. After a 3-d handling period, WM training was performed on 5 consecutive days, with 5 trials per day, which were conducted 2–4 min apart. Memory performance was assessed by measuring the escape latency at each day of training and by the traveled distance at the last training day. For escape latency, we calculated the summed average time of all trials from the start point to attaining one of the platforms. To generate values as robust as possible for individual PS2APP mice, we calculated the z score difference for both methods in contrast to mean WT mouse scores $[(PS2APP - AVG_{WT})/SD_{WT}]$ and built a summed z score for each mouse. On the sixth day, the right platform was placed in the opposite quadrant of the maze to confirm that the mice had used spatial cues rather than rule-based learning to find it. Trials were filmed with a video camera, and the swimming trace was extracted using custom-written LabView software (National Instruments). The experimenter was masked accordingly to the phenotype of the animals.

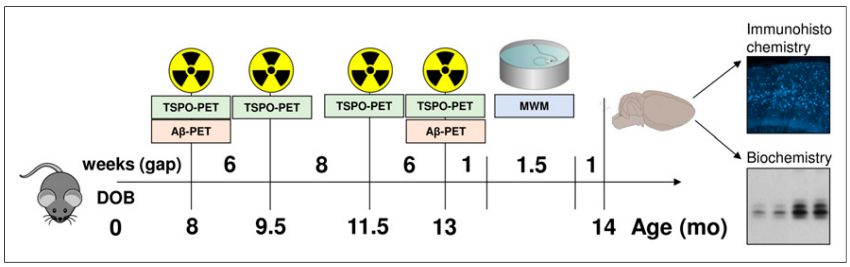

FIGURE 1. Schematic illustration of study design and timeline. We obtained series of dual-tracer PET scans (TSPO and Aβ) in mice between 8 and 13 mo of age. After final scan, we administered behavioral testing by WM, followed by transcardial perfusion with 4% paraformaldehyde and brain extraction for histochemical, immunohistochemical, and biochemical analyses.

Downloaded from jnm.snmjournals.org by on March 26, 2020. For personal use only.

Immunohistochemistry and Biochemistry

Immunohistochemistry in brain regions corresponding to PET was performed for fibrillar Aβ (methoxy-X04), microglia (Iba1), and synaptic density (VGLUT1) as previously established (*25,26*). Soluble Aβ was assessed as previously published (*27*).

Statistics

IBM SPSS Statistics (version 24.0) was used for statistical tests. Normal distribution of data was verified by the Kolmogorov–Smirnov test. Escape latency deriving from the WM test was compared between PS2APP and WT mice by a linear mixed model design including all days of training. Distance values deriving from the last day of training were compared between PS2APP and WT mice by an unpaired Student *t* test. Pearson coefficients of correlation (*R*) were calculated between WM *z* score values of PS2APP mice and their corresponding terminal *z* scores deriving from PET (Aβ and TSPO), immunohistochemistry (Iba1 and methoxy-X04) quantitation, and biochemical levels of soluble Aβ. Voxelwise and VOI-based correlation analyses of baseline and serial PET measures with WM *z* scores were conducted in SPM as described above. VGLUT1 quantification in different brain regions of PS2APP and WT mice was compared by an unpaired Student *t* test. *R* values were calculated for the correlation between WM *z* scores of PS2APP mice and their corresponding VGLUT1 quantification. A threshold *P* value of less than 0.05 was deemed significant for rejection of the null hypothesis.

RESULTS

Microglial Activity, Amyloidosis, and Cognitive Performance in PS2APP Mice

TSPO PET examination of PS2APP mice indicated an inverted U-shape from 8 to 13 mo of age with a peak at 11.5 mo for microglial activation, and Aβ PET showed the expected strong increase in amyloidosis from 8 to 13 mo of age (Figs. 2A and 2B). This increase was most pronounced in the frontal and parietal cortex, as well as in the hippocampus and the thalamus. Microgliosis was strongest in the cortex and the hippocampus but was also strong in subcortical regions devoid of Aβ, such as the striatum and the entorhinal and piriform cortices. Behavioral testing by WM showed that PS2APP mice had cognitive impairment, as revealed by increased escape latency ($F_{(1,15)} = 35.1$, $P < 0.001$) and a 436% higher traveled distance ($P < 0.01$) compared with WT mice (Fig. 2C). There was no difference in speed between PS2APP and WT mice.

Association of Multimodal Terminal Readouts with Cognitive Performance

Next, we asked if terminal readouts of PET or immunohistochemistry correlate with the cognitive performance in PS2APP mice at 13.5 mo of age. The WM performance did not show any correlation with Aβ PET signal in the forebrain or in areas specifically associated with spatial learning 1 wk earlier (both $R < \pm 0.3$; Fig. 3A). On the other hand, there were trends toward better cognitive performance in mice, with the highest TSPO PET signal being in forebrain ($R = -0.46$, $P = 0.18$; Fig. 3A) or in the areas associated with spatial learning ($R = -0.51$, $P = 0.13$). Immunohistochemistry confirmed the in vivo findings: methoxy-X04 quantification of fibrillar Aβ did not indicate an association with cognitive performance ($R < 0.3$; Fig. 3A), whereas quantitation of Iba1 immunostaining showed a significant negative association between microglial activation and WM test scores ($R = -0.77$, $P = 0.01$; Fig. 3A). Multimodal findings in representative mice with good and poor WM performance are illustrated in Figures 3B and 3C.

Furthermore, we saw only a weak correlation between biochemical assays of soluble Aβ and cognitive performance in transgenic mice ($R = -0.36$, $P = 0.30$).

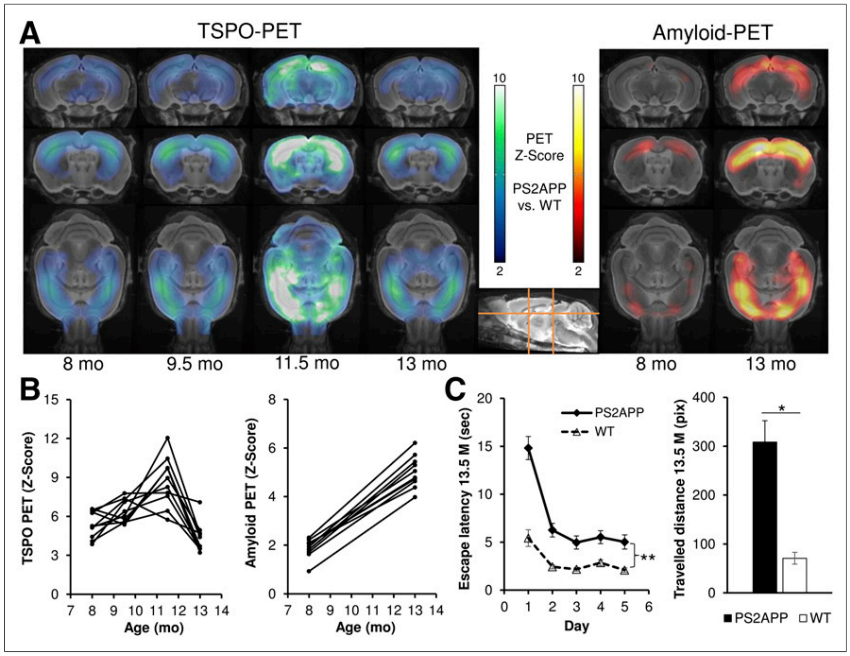

FIGURE 2. Longitudinal TSPO and Aβ PET and performance in behavioral testing. (A) Cortical TSPO PET and Aβ PET signal intensities of PS2APP mice at different ages are expressed as *z* scores relative to findings in age-matched C57BL/6 mice. Coronal and axial slices are projected on T1-weighted MRI template. (B) Progression of individual TSPO PET *z* scores and Aβ PET *z* scores in forebrain of PS2APP mice ($n = 10$) with age. (C) Differences between PS2APP and C57BL/6 (WT) mice for escape latency (sec) and traveled distance in pixels (pix) as WM readouts. Error bars represent SEM. $^*P < 0.01$. $^{**}P < 0.001$.

Prediction of Cognitive Performance by Serial PET Imaging

We undertook longitudinal in vivo observations of amyloidosis and microglial activity by PET to test whether early or cumulative alterations over time of the pathology biomarkers predicted the cognitive outcome of PS2APP mice. We found that better cognitive performance was strongly associated with microglial activation 5 mo earlier in forebrain ($R = -0.71$, $P < 0.05$; Fig. 4A) and especially in cognition-associated areas ($R = -0.82$, $P < 0.01$; Fig. 4B). Peak clusters of the amygdala, the entorhinal cortex, and the hippocampus as identified by SPM gave especially strong regional correlations of high earlier microglial activity and better cognitive performance ($R = -0.95$, $P < 0.001$; Fig. 4C). Statistical maps of the correlation between voxelwise microglial activity and WM performance revealed a pattern, with the strongest association being in brain areas involved in spatial learning networks, that is, the hippocampal formation, the thalamus, and the frontal neocortex (Fig. 4D) (*28*). There were

Downloaded from jnm.snmjournals.org by on March 26, 2020. For personal use only.

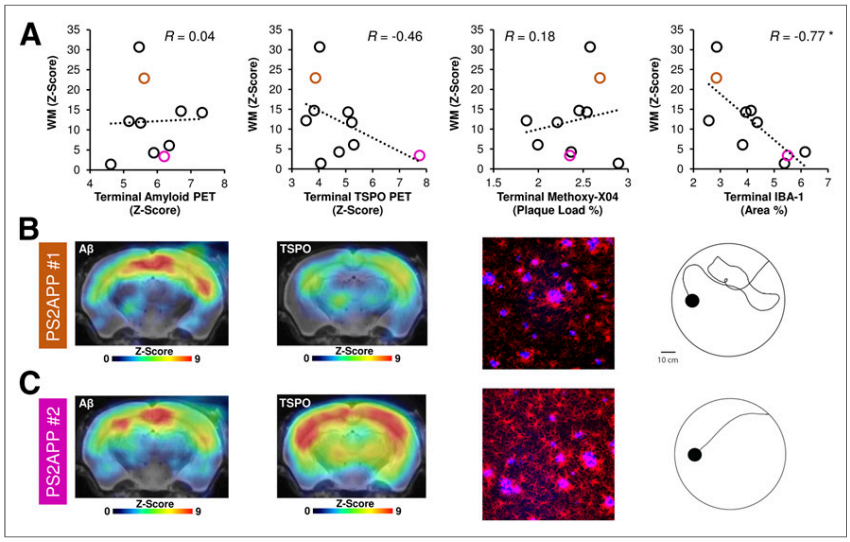

FIGURE 3. Multimodal correlation analysis of cognitive testing with terminal PET and immunohistochemical results in PS2APP mice at study termination. (A) Scatterplots show correlations between individual cognitive testing in WM task (WM, *z* score) with terminal PET and immunohistochemistry readouts. (B and C) Representative PET images (*z* score on MRI template), immunohistochemistry (fused methoxy-X04 [blue] and Iba1 [red]), and WM findings of individual mice, showing either low (B, orange) or high (C, magenta) markers of microglial activation at study termination. Corresponding data points in A are depicted in orange (#1, low markers of microglial activity) and magenta (#2, high markers of microglial activity). *$P < 0.05$.

no brain regions showing a negative correlation between TSPO PET at baseline and better terminal cognitive performance.

We had predicted an opposite relationship for cumulative TSPO PET values over time during the whole 5-mo imaging period, since chronic activation of microglia could damage synapses, leading to neurodegeneration (*7*). However, we still observed the same positive correlation, meaning that high AUCs of microglial activity were associated with a better cognitive performance (Supplemental Figs. 1A–1C; supplemental materials are available at http://jnm.snmjournals.org). Correlations between the AUCs of microglial activity and WM performance were weak when compared with TSPO PET findings at baseline, but the spatial pattern of regions related to spatial learning networks was even better demarcated (Supplemental Fig. 1D). No brain region indicated a significant association between lower longitudinal AUCs of microglial activation and better terminal cognitive performance. There were no relevant associations of the Aβ PET signal at baseline or by longitudinal AUC analysis of amyloidosis with the terminal cognitive performance.

Finally, we asked whether there is a molecular correlate of the associations between microglial activation over time and terminal cognitive performance. Our terminal immunohistochemical analyses of synaptic density showed clear reductions of VGLUT1 in the dentate gyrus and the frontal cortex of PS2APP mice when compared with WT at 14 mo of age (Fig. 5A). Reductions of VGLUT1 in individual PS2APP mice had a moderately strong correlation with behavioral assessment of cognition ($R = -0.53$, $P = 0.12$ each; Fig. 5B). Even more importantly, we also observed that baseline TSPO PET predicted synaptic density measured 5 mo later in the dentate gyrus ($R = 0.71$, $P < 0.05$) and the frontal cortex ($R = 0.57$, $P < 0.1$; Figs. 5B and 5C). Thus, we found that an early microglial response to amyloid pathology in PS2APP transgenic mice protects synaptic density at follow-up.

DISCUSSION

This preclinical investigation exploits the advantages of serial PET for monitoring disease progression in an amyloid transgenic mouse model of AD. For the first time, we report longitudinal TSPO and Aβ PET findings in conjunction with terminal behavioral testing and histologic or biochemical examination to depict associations between longitudinal amyloidosis and neuroinflammation with cognitive outcome in an Aβ/presenilin mouse model of AD. We found that high microglial activation at the onset of amyloidosis predicts for better cognitive performance in PS2APP mice at follow-up 5 mo later, when Aβ pathology is extensive. Interestingly, even longitudinally persistent and terminal elevation of microglial activity was associated with a better cognitive outcome at the end of the trial. On the other hand, early and longitudinal amyloidosis did not predict cognitive outcome and terminal assessments, nor was there any association between amyloidosis and cognition. Multimodal immunohistochemical and biochemical assessments of microglia, amyloidosis, and synaptic density validated and extended the in vivo molecular imaging results.

Neither longitudinal Aβ PET nor terminal immunohistochemistry for detection of fibrillar amyloidosis showed an association with the cognitive performance in individual PS2APP mice. Similarly, quantitative markers of Aβ had only weak correlations with cognition in aged humans (*15*). This seeming dissociation has been attributed to very early onset of fibrillary amyloidosis in AD, with attainment of a plateau level of amyloidosis in most patients by the time that cognitive deterioration has declared itself (*29*). Indeed, soluble fragments of Aβ might be the culprit toxic agents responsible for synaptic damage and cognitive deterioration (*30*), whereas fibrillar Aβ could represent an inert reservoir. Nonetheless, we did not find any correlation between terminal soluble Aβ concentration in brain extracts and cognitive performance in our PS2APP mice at 14 mo of age. Likewise, a recent review of different transgenic mouse models of AD did not find a significant overall correlation between soluble or insoluble levels of Aβ and cognitive function (*31*). In this regard, the brain levels of soluble Aβ may vary over time because of their dynamic turnover, which hampers the interpretation of results obtained at a single time point. We suppose that serial monitoring of soluble Aβ in cerebrospinal fluid over time might reveal more meaningful relationships with the terminal cognitive outcome. The present data do not support a link between progression of amyloidosis to Aβ PET and cognitive performance in individual PS2APP mice, as is in line with the conclusions of the aforementioned review (*31*).

Most importantly, we found a clear benefit of early and longitudinal microglial activation to TSPO PET on the cognitive outcome in this cohort of PS2APP mice (Figs. 3 and 4). This finding in vivo was supported by immunohistochemical analysis showing that the magnitude of synaptic density loss in transgenic mice relative to WT was moderated by an early and ongoing microglial

Downloaded from jnm.snmjournals.org by on March 26, 2020. For personal use only.

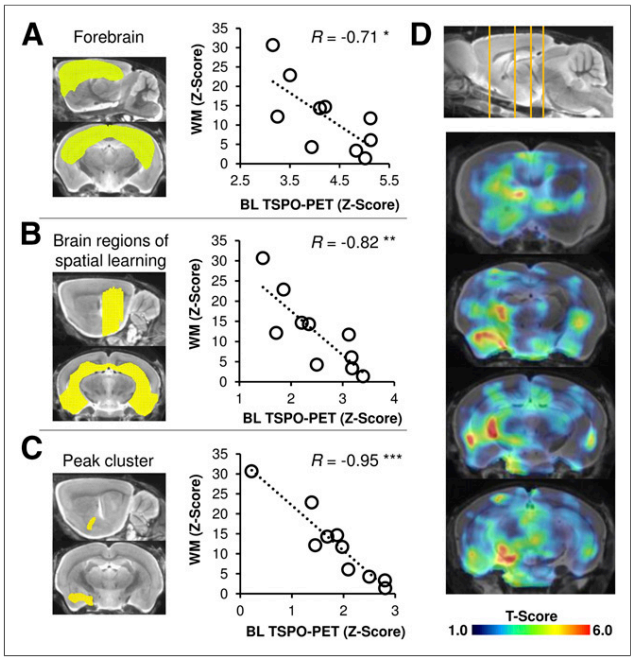

FIGURE 4. Prediction of cognitive performance by magnitude of microglial activation at baseline in PS2APP mice. (A–C) Correlations between individual findings in cognitive testing (*z* scores) with TSPO PET at baseline are presented by scatterplots for forebrain (A), brain regions associated with spatial learning (B), and amygdaloidal peak cluster (C). (D) Coronal slices depict statistical maps (*t* scores) of voxelwise correlation between TSPO PET at baseline (BL) and performance in WM at study termination on T1-weighted MRI template. $^{*}P < 0.05$. $^{**}P < 0.01$. $^{***}P < 0.001$.

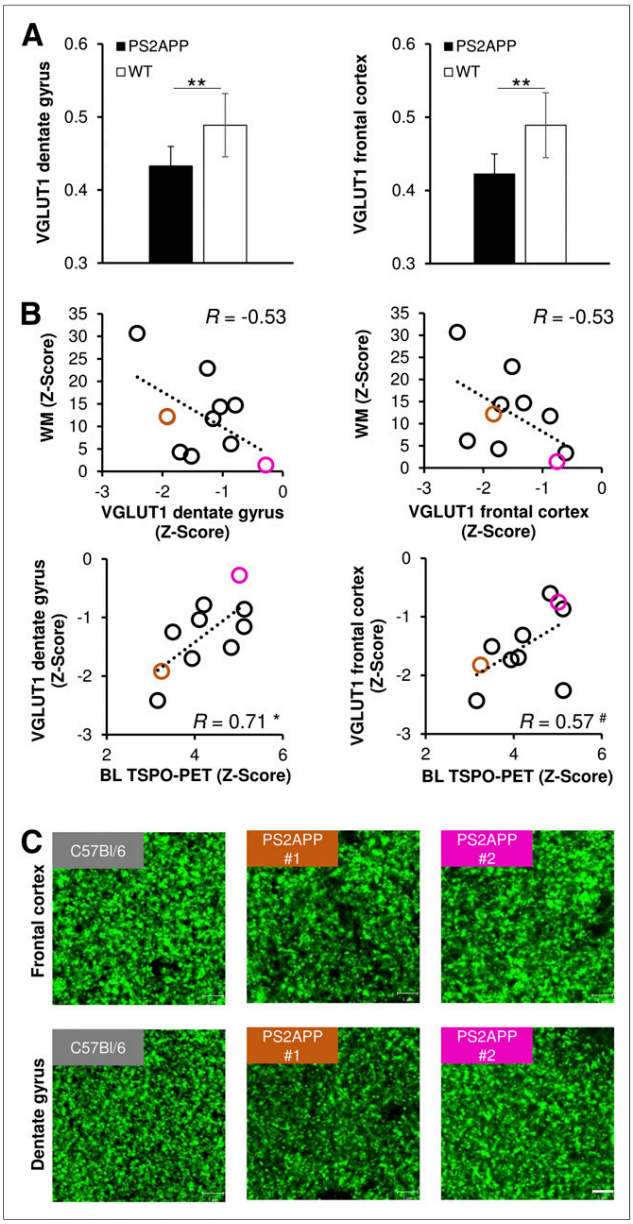

FIGURE 5. Moderation of reductions of synaptic density in PS2APP mice by early microglial response. (A) Reduction in synaptic density (VGLUT1) in PS2APP mice when compared with WT. (B) Scatterplots showing correlation of individual VGLUT1 alterations, cognitive testing, and TSPO PET at baseline in dentate gyrus and frontal cortex of PS2APP mice. (C) Findings of synaptic density (VGLUT1) in representative C57BL/6 WT mouse (gray), together with 2 PS2APP mice, one indicating severe VGLUT1 loss (#1, orange) and other indicating only minor VGLUT1 loss (#2, magenta). Corresponding data points are highlighted in B. Error bars represent SEM. $^{\#}P < 0.1$. $^{*}P < 0.05$. Scale bar represents 5 μm.

response. We also saw some evidence for an association between more pronounced stronger terminal neuroinflammation at 14 mo and better preservation of cognitive function (Fig. 2). At first glance, our findings seem at odds with findings of neuronal dysfunction arising from exposure of neurons to proinflammatory mediators during chronic microglial activation (*7*). However, not all microglia are equal, and it remains a question of specifically which activation state of microglia is actually revealed by an elevated TSPO PET signal or Iba1 immunohistochemistry. In one study, there were some hints that elevated TSPO expression is associated with a CD86-positive proinflammatory microglial phenotype (*32*). Nonetheless, the authors of that study also observed colocalization of TSPO immunostaining with CD206-positive antiinflammatory microglia near amyloid plaques, possibly indicating microglial phagocytosis of toxic Aβ (*33*). Clearance of accumulating debris such as misfolded proteins is indeed a crucial function of antiinflammatory microglia in protecting brain tissue homeostasis (*7*). Interventional studies with, for example, PPARγ agonists to modify microglial phenotype, along with serial microglial monitoring and behavioral testing, might address this question in more detail (*34*). From the current data, it emerges that early microglial activation ameliorates the cognitive decline in PS2APP mice (Fig. 3). Thus, the ability to respond to the developing amyloidosis caused by genetic modification of the mouse model seems an essential aspect of the innate immune system. The net beneficial effect of longitudinal microglial activation on cognitive function might be a matter of duration, as synapses will ultimately suffer from excessive exposure to proinflammatory cytokines. Thus, the present protective effect of elevated microglial activity on cognitive function in PS2APP mice might have turned into deterioration at times after 14 mo.

Another possible explanation for contradictory findings in studies on neuroinflammation and subsequent cognitive outcome might be attributable to differing mechanistic approaches. Most such

Downloaded from jnm.snmjournals.org by on March 26, 2020. For personal use only.

investigations used mice with specific manipulations of genes involved in inflammatory pathways of AD and tested against WT data. We took advantage of the known phenotype heterogeneity of the PS2APP mouse (*35*) to study associations of biomarkers and the terminal cognitive performance in individual mice of the same genotype. Our findings imply that strong microglial activation is probably necessary to cope with the characteristically heavy Aβ deposition in these mice (*14*). This conception fits our current findings of preserved cognitive performance in mice with an early microglial response. As an explanation for this phenomenon, we invoke the recent description of 2 peaks of microglial activation in the time course of human sporadic AD, one occurring in the presymptomatic stage during early amyloid build-up and the other presenting in the dementia stage (*36*). Amyloid mouse models have little neuronal loss and more closely mimic primarily presymptomatic and mild-cognitive-impairment stages of human AD (*27*). Taken together, our preclinical data support the speculation of an early protective peak of microglial activation during initial amyloid aggregation (*36*). Because PS2APP mice show their peak of microglial activation at approximately 11.5 mo (Fig. 1), we speculate that they may lack a second peak, as they do not show much progression of neuronal loss even at very late stages at more than 16 mo of age (*18*).

The main strength of PET lies in its potential to monitor disease-related alterations and interventions over time in an individual. Our present findings are encouraging for longitudinal PET monitoring of microglial activation in human AD, as was recently performed with a first-generation TSPO ligand (*36*). A longitudinal design would enable successive correlation of molecular imaging with cognitive deterioration over time. We suppose that appropriate modulation of microglial activation according to disease stage may lead to interventions with some efficacy. A second main advantage of PET lies in spatial mapping of molecular markers in the whole brain. For the first time, we have generated 3-dimensional maps of microglial activity over time in individual mice (AUC maps) and used these maps for a statistically based voxelwise correlation analysis with cognitive outcome parameters. Statistical testing of SPM-defined regions should be interpreted with care, but our analyses also clearly showed an enhanced association between PET measures of microgliosis in predefined brain regions linked to spatial learning with preserved cognition (*28*). This methodologic innovation provides the basis for designing intervention studies with endpoints relevant to human AD.

CONCLUSION

Early microglial response predicts an improved cognitive outcome in PS2APP mice, whereas the magnitude of fibrillar amyloidosis in early disease stages is not predictive of cognitive performance 5 mo later. These findings emphasize the importance of biomarkers for serial monitoring of microglial activity in AD. Furthermore, the results suggest than the innate immune system could constitute a more relevant therapeutic target than amyloidosis regarding the primary objective of preserving cognitive performance.

DISCLOSURE

Peter Bartenstein and Axel Rominger received speaking honoraria from Piramal Imaging, Laurence Ozmen and Karlheinz Baumann are employees of Hoffmann-La Roche, and Christian Haass is an advisor of Hoffmann-La Roche. Florbetaben precursor was provided by Piramal Imaging. PS2APP mice were provided by F. Hoffmann-La Roche AG. GE Healthcare made GE-180 cassettes available through an early-access model. This work was supported by the Deutsche Forschungsgemeinschaft (DFG) by grants to Matthias Brendel and Axel Rominger (BR4580/1-1 and RO5194/1-1) and within the framework of the Munich Cluster for Systems Neurology (EXC1010SyNergy). No other potential conflict of interest relevant to this article was reported.

ACKNOWLEDGMENTS

We thank Karin Bormann-Giglmaier for excellent technical assistance. We acknowledge Inglewood Biomedical Editing for manuscript editing.

REFERENCES

1. Ziegler-Graham K, Brookmeyer R, Johnson E, Arrighi HM. Worldwide variation in the doubling time of Alzheimer's disease incidence rates. *Alzheimers Dement.* 2008;4:316–323.
2. Heneka MT, Carson MJ, El Khoury J, et al. Neuroinflammation in Alzheimer's disease. *Lancet Neurol.* 2015;14:388–405.
3. McGeer PL, McGeer EG. Mechanisms of cell death in Alzheimer disease: immunopathology. *J Neural Transm Suppl.* 1998;54:159–166.
4. Dansokho C, Heneka MT. Neuroinflammatory responses in Alzheimer's disease. *J Neural Transm.* 2018;125:771–779.
5. Trotta T, Antonietta Panaro M, Cianciulli A, Mori G, Di Benedetto A, Porro C. Microglia-derived extracellular vesicles in Alzheimer's disease: a double-edged sword. *Biochem Pharmacol.* 2018;148:184–192.
6. York EM, Bernier LP, MacVicar BA. Microglial modulation of neuronal activity in the healthy brain. *Dev Neurobiol.* 2018;78:593–603.
7. Heneka MT, Kummer MP, Latz E. Innate immune activation in neurodegenerative disease. *Nat Rev Immunol.* 2014;14:463–477.
8. Hall AM, Roberson ED. Mouse models of Alzheimer's disease. *Brain Res Bull.* 2012;88:3–12.
9. Teipel SJ, Buchert R, Thome J, Hampel H, Pahnke J. Development of Alzheimer-disease neuroimaging-biomarkers using mouse models with amyloid-precursor protein-transgene expression. *Prog Neurobiol.* 2011;95:547–556.
10. Zimmer ER, Leuzy A, Bhat V, Gauthier S, Rosa-Neto P. In vivo tracking of tau pathology using positron emission tomography (PET) molecular imaging in small animals. *Transl Neurodegener.* 2014;3:6.
11. Zimmer ER, Parent MJ, Cuello AC, Gauthier S, Rosa-Neto P. MicroPET imaging and transgenic models: a blueprint for Alzheimer's disease clinical research. *Trends Neurosci.* 2014;37:629–641.
12. Cumming P, Pedersen MD, Minuzzi L, et al. Distribution of PK11195 binding sites in porcine brain studied by autoradiography in vitro and by positron emission tomography. *Synapse.* 2006;59:418–426.
13. Zimmer ER, Leuzy A, Benedet AL, Breitner J, Gauthier S, Rosa-Neto P. Tracking neuroinflammation in Alzheimer's disease: the role of positron emission tomography imaging. *J Neuroinflammation.* 2014;11:120.
14. Brendel M, Probst F, Jaworska A, et al. Glial activation and glucose metabolism in a transgenic amyloid mouse model: a triple-tracer PET study. *J Nucl Med.* 2016;57:954–960.
15. Jagust WJ, Landau SM, Shaw LM, et al. Relationships between biomarkers in aging and dementia. *Neurology.* 2009;73:1193–1199.
16. Knezevic D, Verhoeff NPL, Hafizi S, et al. Imaging microglial activation and amyloid burden in amnestic mild cognitive impairment. *J Cereb Blood Flow Metab.* January 1, 2017 [Epub ahead of print].
17. Brendel M, Jaworska A, Herms J, et al. Amyloid-PET predicts inhibition of de novo plaque formation upon chronic gamma-secretase modulator treatment. *Mol Psychiatry.* 2015;20:1179–1187.
18. Ozmen L, Albientz A, Czech C, Jacobsen H. Expression of transgenic APP mRNA is the key determinant for beta-amyloid deposition in PS2APP transgenic mice. *Neurodegener Dis.* 2009;6:29–36.
19. Richards JG, Higgins GA, Ouagazzal AM, et al. PS2APP transgenic mice, coexpressing hPS2mut and hAPPswe, show age-related cognitive deficits associated

Downloaded from jnm.snmjournals.org by on March 26, 2020. For personal use only.

with discrete brain amyloid deposition and inflammation. *J Neurosci.* 2003;23:8989–9003.
20. Overhoff F, Brendel M, Jaworska A, et al. Automated spatial brain normalization and hindbrain white matter reference tissue give improved [^{18}F]-florbetaben PET quantitation in Alzheimer's model mice. *Front Neurosci.* 2016;10:45.
21. Deussing M, Blume T, Vomacka L, et al. Coupling between physiological TSPO expression in brain and myocardium allows stabilization of late-phase cerebral [^{18}F]GE180 PET quantification. *Neuroimage.* 2018;165:83–91.
22. Sauvage M, Brabet P, Holsboer F, Bockaert J, Steckler T. Mild deficits in mice lacking pituitary adenylate cyclase-activating polypeptide receptor type 1 (PAC1) performing on memory tasks. *Brain Res Mol Brain Res.* 2000;84:79–89.
23. Busche MA, Kekus M, Adelsberger H, et al. Rescue of long-range circuit dysfunction in Alzheimer's disease models. *Nat Neurosci.* 2015;18:1623–1630.
24. Keskin AD, Kekus M, Adelsberger H, et al. BACE inhibition-dependent repair of Alzheimer's pathophysiology. *Proc Natl Acad Sci USA.* 2017;114:8631–8636.
25. Brendel M, Focke C, Blume T, et al. Time courses of cortical glucose metabolism and microglial activity across the life span of wild-type mice: a PET study. *J Nucl Med.* 2017;58:1984–1990.
26. Dorostkar MM, Dreosti E, Odermatt B, Lagnado L. Computational processing of optical measurements of neuronal and synaptic activity in networks. *J Neurosci Methods.* 2010;188:141–150.
27. Brendel M, Kleinberger G, Probst F, et al. Increase of TREM2 during aging of an Alzheimer's disease mouse model is paralleled by microglial activation and amyloidosis. *Front Aging Neurosci.* 2017;9:8.
28. D'Hooge R, De Deyn PP. Applications of the Morris water maze in the study of learning and memory. *Brain Res Brain Res Rev.* 2001;36:60–90.
29. Jack CR Jr, Holtzman DM. Biomarker modeling of Alzheimer's disease. *Neuron.* 2013;80:1347–1358.
30. Willem M, Tahirovic S, Busche MA, et al. η-secretase processing of APP inhibits neuronal activity in the hippocampus. *Nature.* 2015;526:443–447.
31. Foley AM, Ammar ZM, Lee RH, Mitchell CS. Systematic review of the relationship between amyloid-beta levels and measures of transgenic mouse cognitive deficit in Alzheimer's disease. *J Alzheimers Dis.* 2015;44:787–795.
32. Liu B, Le KX, Park MA, et al. In vivo detection of age- and disease-related increases in neuroinflammation by ^{18}F-GE180 TSPO microPET imaging in wild-type and Alzheimer's transgenic mice. *J Neurosci.* 2015;35:15716–15730.
33. Yamanaka M, Ishikawa T, Griep A, Axt D, Kummer MP, Heneka MT. PPARgamma/RXRalpha-induced and CD36-mediated microglial amyloid-beta phagocytosis results in cognitive improvement in amyloid precursor protein/presenilin 1 mice. *J Neurosci.* 2012;32:17321–17331.
34. Zou C, Shi Y, Ohli J, Schuller U, Dorostkar MM, Herms J. Neuroinflammation impairs adaptive structural plasticity of dendritic spines in a preclinical model of Alzheimer's disease. *Acta Neuropathol.* 2016;131:235–246.
35. Brendel M, Jaworska A, Griessinger E, et al. Cross-sectional comparison of small animal [^{18}F]-florbetaben amyloid-PET between transgenic AD mouse models. *PLoS One.* 2015;10:e0116678.
36. Fan Z, Brooks DJ, Okello A, Edison P. An early and late peak in microglial activation in Alzheimer's disease trajectory. *Brain.* 2017;140:792–803.

Erratum

In the article "Intraindividual Comparison of ^{18}F-PSMA-1007 PET/CT, Multiparametric MRI, and Radical Prostatectomy Specimens in Patients with Primary Prostate Cancer: A Retrospective, Proof-of-Concept Study" by Kesch et al. (*J Nucl Med.* 2017;58:1805–1810), the reported sensitivities, specificities, and positive and negative predictive values for mpMRI and the ^{18}F-PSMA-1007 PET/CT combination are not correct due to a systematic calculation error. The correct values appear in italics in the paragraphs as well as the table below. Despite these errors, the main conclusions have not changed. The authors regret the error.

In the abstract:

^{18}F-PSMA-1007 PET/CT had an NPV of 68% and accuracy of 75%, and mpMRI had an NPV of *63%* and accuracy of 73% for total agreement. Near-total agreement analysis resulted in an NPV of *83%* and an accuracy of 93% for 18F-PSMA-1007 PET/CT and 91% and 87% for mpMRI, respectively.

In the "Results" section:

MpMRI had *60%* sensitivity, *88%* specificity, *86%* PPV, *64%* NPV, and accuracy of 73% for total agreement and *85%* sensitivity, *91%* specificity, *92%* PPV, *83%* NPV, and accuracy of 87% for near-total agreement. The combination of ^{18}F-PSMA-1007-PET/CT and mpMRI had *85%* sensitivity, *75%* specificity, *81%* PPV, *81%* NPV, and accuracy of 81% for total agreement and *99%* sensitivity, *85%* specificity, *89%* PPV, *99%* NPV, and accuracy of 93% for near-total agreement (Table 2).

Subsequently, we stated in the *"Discussion" section* on page 1809, "Compared with mpMRI, ^{18}F-PSMA-1007 . . . had a worse sensitivity and NPV for total agreement." However, ^{18}F-PSMA-1007 had a *worse specificity* for total agreement.

TABLE 2

Agreement	Sensitivity	Specificity	PPV	NPV	Accuracy
Total					
^{18}F-PSMA-1007 PET/CT	71% (64%–77%)	81% (75%–87%)	83% (77%–88%)	68% (61%–75%)	75%
mpMRI	*60% (52%–67%)*	*88% (82%–93%)*	*86% (79%–92%)*	*64% (57%–71%)*	73%
Combination	*85% (79%–90%)*	*75% (68%–82%)*	*81% (75%–86%)*	*81% (73%–87%)*	81%
Near-total					
^{18}F-PSMA-1007 PET/CT	93% (89%–96%)	92% (87%–96%)	94% (90%–97%)	91% (86%–95%)	93%
mpMRI	*85% (79%–90%)*	*91% (85%–95%)*	*92% (87%–96%)*	*83% (76%–88%)*	87%
Combination	*99% (96%–100%)*	*85% (78%–90%)*	*89% (84%–93%)*	*99% (95%–100%)*	93%

Data in parentheses are 95% CIs.

Downloaded from jnm.snmjournals.org by on March 26, 2020. For personal use only.

JNM The Journal of NUCLEAR MEDICINE

^{68}Ga-FAPI PET/CT: Tracer Uptake in 28 Different Kinds of Cancer

Clemens Kratochwil, Paul Flechsig, Thomas Lindner, Labidi Abderrahim, Annette Altmann, Walter Mier, Sebastian Adeberg, Hendrik Rathke, Manuel Röhrich, Hauke Winter, Peter K. Plinkert, Frederik Marme, Matthias Lang, Hans-Ulrich Kauczor, Dirk Jäger, Jürgen Debus, Uwe Haberkorn and Frederik L. Giesel

J Nucl Med. 2019;60:801-805.
Published online: April 6, 2019.
Doi: 10.2967/jnumed.119.227967

This article and updated information are available at:
http://jnm.snmjournals.org/content/60/6/801

Information about reproducing figures, tables, or other portions of this article can be found online at:
http://jnm.snmjournals.org/site/misc/permission.xhtml

Information about subscriptions to JNM can be found at:
http://jnm.snmjournals.org/site/subscriptions/online.xhtml

The Journal of Nuclear Medicine is published monthly.
SNMMI | Society of Nuclear Medicine and Molecular Imaging
1850 Samuel Morse Drive, Reston, VA 20190.
(Print ISSN: 0161-5505, Online ISSN: 2159-662X)

© Copyright 2019 SNMMI; all rights reserved.

SNMMI SOCIETY OF NUCLEAR MEDICINE AND MOLECULAR IMAGING

Downloaded from jnm.snmjournals.org by on March 26, 2020. For personal use only.

^{68}Ga-FAPI PET/CT: Tracer Uptake in 28 Different Kinds of Cancer

Clemens Kratochwil*[1], Paul Flechsig*[1,2], Thomas Lindner[1], Labidi Abderrahim[1], Annette Altmann[1,3], Walter Mier[1], Sebastian Adeberg[4,5], Hendrik Rathke[1], Manuel Röhrich[1], Hauke Winter[2,6], Peter K. Plinkert[7], Frederik Marme[8,9], Matthias Lang[10], Hans-Ulrich Kauczor[2,11], Dirk Jäger[12,13], Jürgen Debus[4,5,14], Uwe Haberkorn[1–3], and Frederik L. Giesel[1]

*[1]Department of Nuclear Medicine, University Hospital Heidelberg, Heidelberg, Germany; [2]Translational Lung Research Center Heidelberg, German Center for Lung Research, Heidelberg, Germany; [3]Clinical Cooperation Unit Nuclear Medicine, German Cancer Research Center, Heidelberg, Germany; [4]Department of Radiation Oncology, University Hospital Heidelberg, Heidelberg, Germany; [5]Heidelberg Institute for Radiation Oncology, Heidelberg, Germany; [6]Department of Surgery, Thoraxklinik at University Hospital Heidelberg, Heidelberg, Germany; [7]Department of Otorhinolaryngology, Head and Neck Surgery, University Hospital Heidelberg, Heidelberg, Germany; [8]Department Obstetrics and Gynecology, University Hospital Heidelberg, Heidelberg, Germany; [9]Department Obstetrics and Gynecology, University Hospital Mannheim, Mannheim, Germany; [10]Department of Surgery, University Hospital Heidelberg, Heidelberg, Germany; [11]Department of Diagnostic and Interventional Radiology, University Hospital Heidelberg, Heidelberg, Germany; [12]Department of Medical Oncology and Internal Medicine VI, National Center for Tumor Diseases, University Hospital Heidelberg, Germany; [13]Clinical Cooperation Unit Applied Tumor Immunity, German Cancer Research Center, Heidelberg, Germany; and [14]Clinical Cooperation Unit Radiation Oncology, German Cancer Research Center, Heidelberg, Germany

The recent development of quinoline-based PET tracers that act as fibroblast-activation-protein inhibitors (FAPIs) demonstrated promising preclinical and clinical results. FAP is overexpressed by cancer-associated fibroblasts of several tumor entities. Here, we quantify the tumor uptake on ^{68}Ga-FAPI PET/CT of various primary and metastatic tumors to identify the most promising indications for future application. **Methods:** ^{68}Ga-FAPI PET/CT scans were requested by various referring physicians according to individual clinical indications that were considered insufficiently covered by ^{18}F-FDG PET/CT or other imaging modalities. All PET/CT was performed 1 h after injection of 122–312 MBq of ^{68}Ga-FAPI-04. We retrospectively identified 80 patients with histopathologically proven primary tumors or metastases or radiologically unequivocal metastatic lesions of histologically proven primary tumors. Tumor uptake was quantified by SUV_{max} and SUV_{mean} (60% isocontour). **Results:** Eighty patients with 28 different tumor entities (54 primary tumors and 229 metastases) were evaluated. The highest average SUV_{max} (>12) was found in sarcoma, esophageal, breast, cholangiocarcinoma, and lung cancer. The lowest ^{68}Ga-FAPI uptake (average SUV_{max} < 6) was observed in pheochromocytoma, renal cell, differentiated thyroid, adenoid cystic, and gastric cancer. The average SUV_{max} of hepatocellular, colorectal, head–neck, ovarian, pancreatic, and prostate cancer was intermediate (SUV 6–12). SUV varied across and within all tumor entities. Because of low background in muscle and blood pool (SUV_{max} < 2), the tumor-to-background contrast ratios were more than 3-fold in the intermediate and more than 6-fold in the high-intensity uptake group. **Conclusion:** Several highly prevalent cancers presented with remarkably high uptake and image contrast on ^{68}Ga-FAPI PET/CT. The high and rather selective tumor uptake may open up new applications for noninvasive tumor characterization, staging examinations, or radioligand therapy.

Key Words: FAPI; breast cancer; colorectal cancer; lung cancer; PET/CT

J Nucl Med 2019; 60:801–805
DOI: 10.2967/jnumed.119.227967

Several tumor entities, such as breast, colon, and pancreatic carcinomas, are characterized by a strong desmoplastic reaction (*1*). Cancer-associated fibroblasts and extracellular fibrosis can contribute up to 90% of the gross tumor mass, leaving original tumor cells in the minority (*2,3*). Many cancer-associated fibroblasts differ from normal fibroblasts by their relative specific expression of fibroblast activation protein (FAP). Therefore, FAP-specific inhibitors were first developed as anticancer drugs and then were consecutively advanced into tumor-targeting radiopharmaceuticals (*4,5*).

A biodistribution and initial dosimetry study of ^{68}Ga-FAP inhibitor (FAPI) PET/CT with 2 DOTA-containing ligands suggested that these tracers may expand and enrich the diagnostic cancer portfolio currently covered by ^{18}F-FDG (*6*). Moreover, the biodistribution suggested that ^{68}Ga-FAPI may be suitable for radioligand therapy (*7*). In view of the favorable initial results, ^{68}Ga-FAPI PET/CT was requested by various referring physicians on the basis of individual clinical indications. Often, scans were ordered to improve tumor delineation for planned surgery or radiotherapy. Thus, even lesions that were already unequivocally identified radiologically or by histopathology could be additionally characterized with ^{68}Ga-FAPI PET/CT.

The aim of this retrospective analysis was to quantify ^{68}Ga-FAPI uptake in a variety of primary, metastatic, or recurring cancers.

Received Mar. 5, 2019; revision accepted Mar. 19, 2019.
For correspondence or reprints contact: Clemens Kratochwil, Department of Nuclear Medicine, University Hospital Heidelberg, Im Neuenheimer Feld 400, 69120 Heidelberg, Germany.
E-mail: clemens.kratochwil@med.uni-heidelberg.de
*Contributed equally to this work.
Published online Apr. 6, 2019.
COPYRIGHT © 2019 by the Society of Nuclear Medicine and Molecular Imaging.

Downloaded from jnm.snmjournals.org by on March 26, 2020. For personal use only.

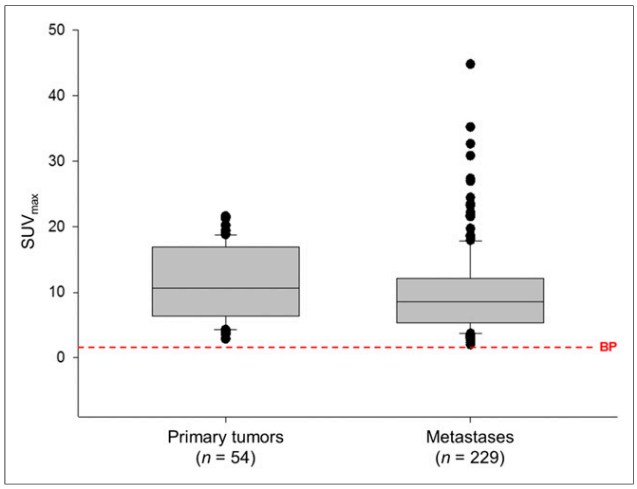

FIGURE 1. Neither mean, median, nor range of SUV_{max} of ^{68}Ga-FAPI-04 PET differs significantly between primary tumors and metastases.

MATERIALS AND METHODS

Patients

All patients were referred for experimental diagnostics by their treating oncologists, who were facing an unmet diagnostic challenge that could not be solved sufficiently with standard diagnostic means. Although the location and nature of tumor lesions were frequently known, the intent was to improve tumor delineation for reasons such as planning of radiotherapy. All patients gave written informed consent to receive ^{68}Ga-FAPI PET/CT on an individual-patient basis. The data were analyzed retrospectively with approval of the local ethics committee (approval S016/2018).

Radiopharmaceuticals

Synthesis and labeling of ^{68}Ga-FAPI-04 have already been described previously (*4,5*). Following the regulations of the German Pharmaceuticals Act §13(2b), the indication for the exam and labeling of the FAPI tracers was done under the direct responsibility of the applying physician. Injected activities were dependent on labeling yields. According to a previous dosimetry estimate—effective dose, 1.6 mSv/100 MBq (*6*)—an upper limit of 370 MBq regarding radiation exposure and a lower limit of 100 MBq per examination to achieve a sufficient count rate have been considered.

PET/CT Imaging

All imaging was performed on a Biograph mCT Flow scanner (Siemens). After non–contrast-enhanced low-dose CT (130 keV, 30 mAs, CareDose; reconstructed with a soft-tissue kernel to a slice thickness of 5 mm), PET was acquired in 3-dimensional mode (matrix, 200 × 200) using FlowMotion (Siemens). The emission data were corrected for randoms, scatter, and decay. Reconstruction was performed with an ordered-subset expectation maximization algorithm with 2 iterations/21 subsets and was Gauss-filtered to a transaxial resolution of 5 mm in full width at half maximum; attenuation correction was performed using the nonenhanced low-dose CT data. The injected activity for the ^{68}Ga-FAPI examinations was 122–312 MBq, and the PET scans were started 1 h after injection. A 500-mL volume of saline with 20 mg of furosemide was infused from 15 min before to 30 min after tracer application. The patients were asked to self-report any abnormalities 30 min after finishing the examination.

Imaging Evaluation

Tumor tracer uptake was quantified by SUV_{mean} and SUV_{max} at 1 h after injection. For calculation of the SUV, circular regions of interest were drawn around the tumor lesions with focally increased uptake in transaxial slices and automatically adapted to a 3-dimensional volume of interest with e.soft software (Siemens) at a 60% isocontour. The unspecific background in blood pool (aortic vessel content) and muscle was quantified with a circular 2-cm-diameter sphere.

RESULTS

Adverse Events

All patients tolerated the examination well. No drug-related pharmacologic effects or physiologic responses occurred. During injection and the 1.5 h of follow-up, no patient reported any new symptoms.

Quantifying ^{68}Ga-FAPI Uptake in Primary Tumors and Metastatic Disease

Patient numbers were not sufficient to compare the SUVs of primary tumors versus metastases for individual cancers. The overall SUV mean (11.5 ± 5.5 vs. 10.0 ± 6.3), median (10.7 vs. 8.5), and range (2.9–21.6 vs. 2.0–44.8) of ^{68}Ga-FAPI in primary tumors (n = 54) and metastatic lesions (n = 229) did not differ (Fig. 1). Subsequently, we analyzed primary and metastatic lesions of individual tumor entities in a pooled fashion.

The highest average SUV_{max} (>12) was found in sarcoma, esophageal, breast, cholangiocarcinoma, and lung cancer. The lowest ^{68}Ga-FAPI uptake (average SUV_{max} < 6) was observed in renal cell, differentiated thyroid, adenoid cystic, gastric, and pheochromocytoma cancer. The average SUV_{max} of hepatocellular, colorectal, head–neck, ovarian, pancreatic, and prostate cancer was

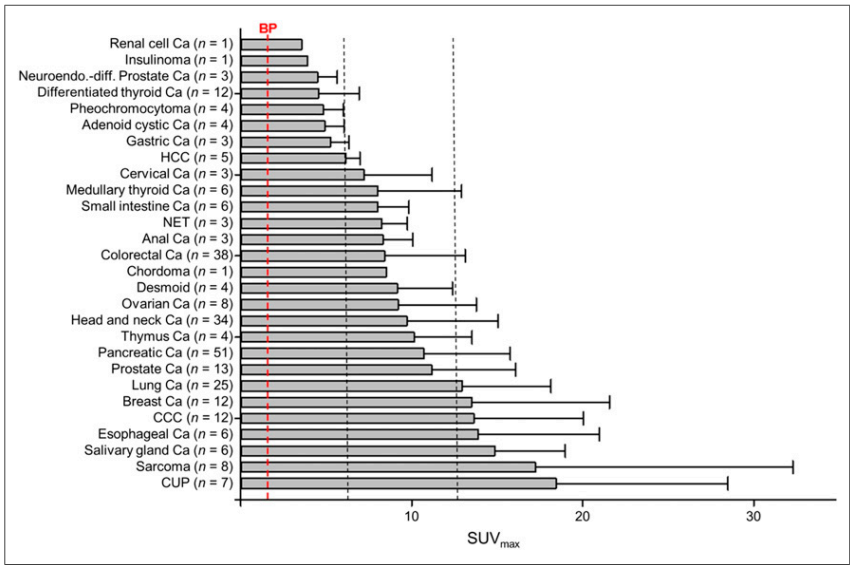

FIGURE 2. Average SUV_{max} of ^{68}Ga-FAPI PET/CT in various tumor entities. Low, intermediate, and high uptake was defined by cutoff at SUVs 6 and 12. By comparison, average background (blood pool) was found to have SUV 1.4. Ca = cancer; CCC = cholangiocellular carcinoma; CUP = carcinoma of unknown primary; HCC = hepatocellular carcinoma; NET = neuroendocrine tumor.

Downloaded from jnm.snmjournals.org by on March 26, 2020. For personal use only.

intermediate (SUV 6–12). All tumor entities exhibited a high interindividual SUV variation (Fig. 2). Because of the low background activity (average SUV_{mean} of blood pool and muscle, 1.2 and 1.0, respectively; SUV_{max}, 1.6 and 1.4, respectively), the tumor-to-background ratios are more than 3 in the intermediate and more than 6 in the high-intensity uptake group (Fig. 2). These high ratios resulted in high image contrast and excellent tumor delineation in most of the evaluated patients (Fig. 3).

DISCUSSION

The aim of this retrospective analysis was to quantify the uptake of ^{68}Ga-FAPI ligand in different types of cancer.

The highest uptake (average $SUV_{max} > 12$) was found in lung, breast, and esophageal cancer; cholangiocellular carcinoma; and sarcoma. This may open indications for ^{68}Ga-FAPI PET/CT for cases in which ^{18}F-FDG PET/CT faces its limitations. Because of low uptake of ^{18}F-FDG in low-grade sarcomas, there is a wide overlap between benign and malignant lesions, and even dual–time-point imaging could not eliminate this well-known limitation of ^{18}F-FDG PET/CT (*8,9*). The main limitation of ^{18}F-FDG PET/CT in staging of esophageal cancer is its low to moderate sensitivity for lymph node staging (*10*) and delineation between viable tumor and regional esophagitis. In breast cancer, ^{18}F-FDG PET/CT is commonly used in recurrence but not generally recommended for initial staging (*11*). Cholangiocarcinoma exhibits considerable variability in ^{18}F-FDG uptake, which was correlated with a weak expression of hexokinase-2 (*12*). ^{18}F-FDG PET/CT performs well in lung cancer; however, high cerebral background requires brain MRI for complete staging (*13*). Thus, these tumors may benefit from ^{68}Ga-FAPI PET/CT imaging. However, the limited number of patients examined by ^{68}Ga-FAPI PET/CT until now does not allow subgroup analysis of histologic variants or differentiation grades.

Surprisingly, colon and pancreatic cancers, that is, the ones with the highest desmoplastic reaction by histopathology (*3*), demonstrated only intermediate ^{68}Ga-FAPI uptake (SUV 6–12). The liver is the first target organ for metastases of colorectal cancer. We already reported a significantly lower hepatic background for ^{68}Ga-FAPI (SUV 1.7) than for ^{18}F-FDG (SUV 2.8). This may be advantageous for liver metastasis detection (*6*). Within the patients reported here, we identified liver metastases as small as 1 cm in diameter (Fig. 4). Because of its limited sensitivity of 30% for detecting lymph node metastasis (*14*) and false-positive findings in acute pancreatitis, ^{18}F-FDG PET is of limited usefulness for surgical planning in pancreatic cancer (*15*). Thus, even intermediate uptake in ^{68}Ga-FAPI PET/CT presents a reasonable perspective to improve clinical diagnostic performance. In ovarian cancer, another tumor in the intermediate-intensity group, ^{18}F-FDG can overcome some limits of conventional imaging but, because of peristaltic activity, often suffers from heterogeneous uptake in the intestinal wall (*16,17*). In contrast, ^{68}Ga-FAPI demonstrates very low unspecific intestinal/peritoneal uptake and might be superior to identify peritoneal carcinomatosis, the main clinical challenge of advanced-stage ovarian cancer. Head–neck tumors often go along with local inflammation. Unfortunately, a recent review reported that most original work found that ^{18}F-FDG PET/CT is not useful in discriminating benign from malignant tumors because of the overlap of uptake in both conditions (*18–20*). In this setting, ^{68}Ga-FAPI PET/CT may offer an advantage regarding tumor delineation—for example, in planning of radiotherapy (Fig. 5). Differentiation between residual/recurrent disease and postchemoradiation fibrosis was reported to be a diagnostic challenge for ^{18}F-FDG (*21*). It should be mentioned that unspecific fibrosis may also cause issues for ^{68}Ga-FAPI PET; however, because of the inherent difference in normal activated fibroblasts and cancer-associated fibroblasts (*4,5*), this possibility

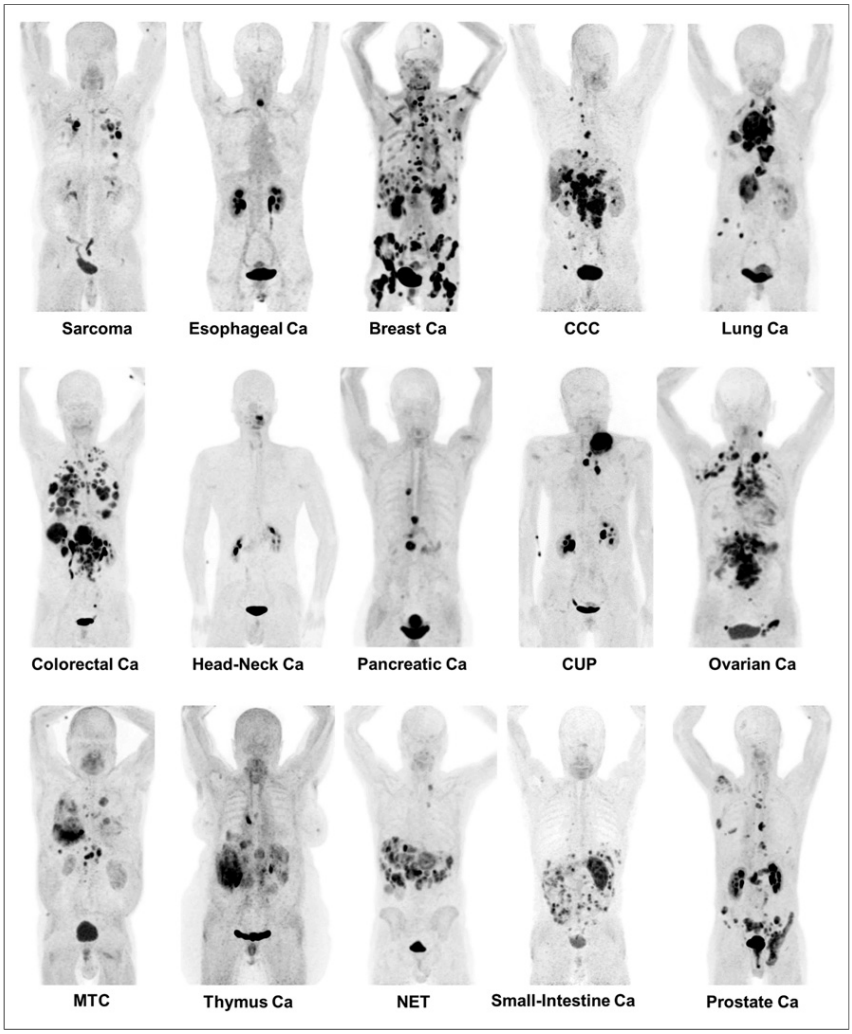

FIGURE 3. Maximum-intensity projections of ^{68}Ga-FAPI PET/CT in patients reflecting 15 different histologically proven tumor entities (sorted by uptake in descending order). Ca = cancer; CCC = cholangiocellular carcinoma; CUP = carcinoma of unknown primary; MTC = medullary thyroid cancer; NET = neuroendocrine tumor.

Downloaded from jnm.snmjournals.org by on March 26, 2020. For personal use only.

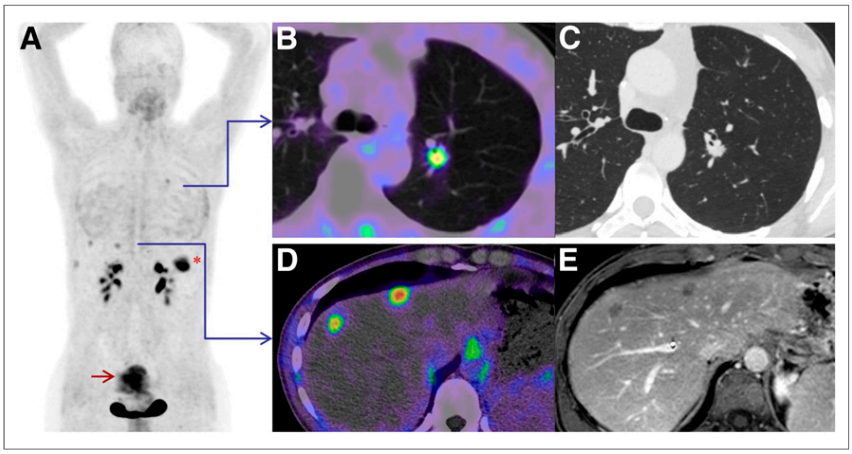

FIGURE 4. Maximum-intensity projection (A) of patient with colorectal carcinoma. Because of low physiologic background uptake, tiny lesions in lung (B) and liver (D) were detected by ^{68}Ga-FAPI-04 PET/CT and measured in dedicated CT of lung (C) and hepatic MRI (E) with long-axis diameters of 1 cm. *Primary tumor in left colon flexure. Red arrow = unspecific uptake in uterus.

still needs to be proven. Intermediate to high ^{68}Ga-FAPI uptake was also observed in prostate cancer. However, only patients with prostate-specific membrane antigen–negative tumors, which are the minority of prostate cancers, were selected to receive additional ^{68}Ga-FAPI PET/CT, and because of this selection bias, our cohort does not reflect typical patients.

^{18}F-FDG PET often performs poorly in renal cell carcinoma, pheochromocytoma, and neuroendocrine tumors, including medullary thyroid cancer and insulinomas. This limitation is unlikely to be overcome, because SUVs for these tumors are also low for ^{68}Ga-FAPI (average $SUV_{max} < 6$). This is likely not a significant problem because several special PET tracers such as ^{18}F-DOPA for neuroblastoma/pheochromocytoma (*22*), ^{68}Ga-labeled somatostatin analogs for neuroendocrine tumors (*23*), ^{89}Zr-girentuximab for renal cell carcinoma (*24*), and ^{68}Ga-exendin targeting glucagon-like peptide-1 receptor on insulinoma (*25*) recently closed this gap.

The current imaging findings are largely consistent with histopathology reports. FAP expression on activated fibroblasts in tumor stroma was already quantified in 1990 using the antibody-F19 (*3*). Well in line with our results, a weak desmoblastic reaction was observed in renal cell cancer and neuroblastoma/pheochromocytoma; intermediate staining in pancreatic, gastric, endometrial/cervix cancer; and high expression in breast cancer (*3*). In contrast to this historical paper, we found a higher ^{68}Ga-FAPI uptake in neuroendocrine tumors (intermediate group in ^{68}Ga-FAPI PET, weak in histology) and lung cancer (high uptake in ^{68}Ga-FAPI PET, intermediate in histology). For colorectal cancer, which was the most commonly high-expressing tumor in the work of Garin-Chesa et al. (*3*), we only measured intermediate values. Low case numbers, heterogeneity of expression, random effects in tissue sampling, and high interindividual variability appear the most appropriate explanations for these differences between histologic in vitro and imaging in vivo results. Another explanation and also a possible reason for the high interindividual variability can be patient selection. Immunohistochemical work-up has primarily been performed in early-stage nonmetastatic, and thus rather indolent, tumors. In contrast, the patients evaluated by ^{68}Ga-FAPI PET/CT are a more heterogeneous group. Most presented with recurrent and metastatic disease and sometimes (most frequently in colorectal cancer patients) even after several lines of systemic therapy. We also want to emphasize that the aim of this work was only to characterize true-positive lesions (proven by histopathology or unequivocal radiologic findings of histopathologically proven primary tumors), as no acceptable gold standard to rule out false-negative findings was available. Thus, sensitivity and overall diagnostic accuracy cannot be determined.

FAP was considered a promising target for nuclear-labeled tumor probes in 1994. Because of tumor-to-liver ratios of up to 21:1, the antibody ^{131}I-mAb-F19 could delineate liver metastases of colorectal cancer as small as 1 cm in diameter (*26*). This was confirmed by our observations (Fig. 4) and is supported by earlier data that cancer-associated fibroblasts are already found in lesions above 1–2 mm in diameter (*27*). However, well in line with typical antibody kinetics, the optimal time for tumor imaging with ^{131}I-mAb-F19 was 3–5 d after administration (*26*). In contrast, ^{68}Ga-FAPI PET/CT can be performed 10 min to 1 h after administration and, in contrast to ^{18}F-FDG studies, can be done without fasting and resting time (*6*). This is a potential operational advantage, as observed between prostate-specific membrane antigen targeting with the antibody J591 and an optimal imaging after 6–8 d (*28*) versus low-molecular-weight prostate-specific membrane antigen ligands that can be imaged 1 h after injection (*29*).

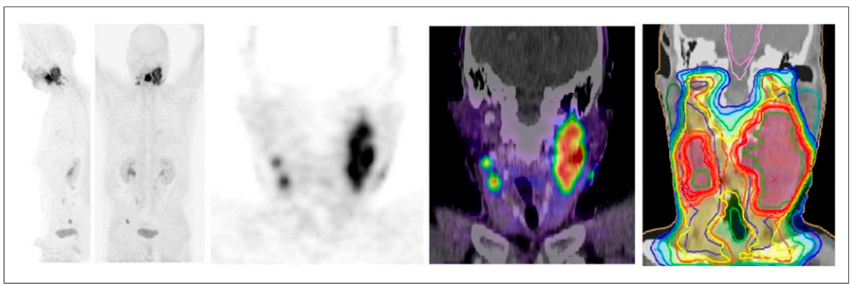

FIGURE 5. Among others, one clinical application for ^{68}Ga-FAPI PET/CT can be to improve gross tumor volume delineation in preparation for external-beam radiotherapy—in this case, squamous cell carcinoma of neck with local lymph node metastases. From left to right: whole-body maximum-intensity projections, coronal PET slice through head/neck tumor, its fusion with coregistered CT, PET-segmented target-volume definition for external-beam radiotherapy.

CONCLUSION

Several epidemiologically important tumor entities, in particular breast, esophagus, lung, pancreatic, head–neck, and colorectal cancer, present with a remarkably high uptake in ^{68}Ga-FAPI PET/CT. This may open new applications for noninvasive tumor characterization and staging examinations. Because the ^{68}Ga-FAPI tracers contain the universal DOTA chelator, also a theranostic approach—after labeling the ligand with an appropriate therapeutic radionuclide—seems feasible. Other known ^{18}F-FDG limitations, for example, in differentiated thyroid

Downloaded from jnm.snmjournals.org by on March 26, 2020. For personal use only.

and renal cell carcinoma, can probably not be overcome with ^{68}Ga-FAPI. The limitations of this report, such as retrospective evaluation, a heterogeneous patient collective, and a low case number for some kinds of tumor, require further studies.

DISCLOSURE

A patent application for quinoline-based FAP-targeting agents for imaging and therapy in nuclear medicine presents a potential financial conflict of interest for authors Clemens Kratochwil, Thomas Lindner, Walter Mier, Uwe Haberkorn, and Frederik Giesel. No other potential conflict of interest relevant to this article was reported.

REFERENCES

1. Siveke JT. Fibroblast-activating protein: targeting the roots of the tumor microenvironment. *J Nucl Med.* 2018;59:1412–1414.
2. Hamson EJ, Keane FM, Tholen S, Schilling O, Gorrell MD. Understanding fibroblast activation protein (FAP): substrates, activities, expression and targeting for cancer therapy. *Proteomics Clin Appl.* 2014;8:454–463.
3. Garin-Chesa P, Old LJ, Rettig WJ. Cell surface glycoprotein of reactive stromal fibroblasts as a potential antibody target in human epithelial cancers. *Proc Natl Acad Sci USA.* 1990;87:7235–7239.
4. Loktev A, Lindner T, Mier W, et al. A tumor-imaging method targeting cancer-associated fibroblasts. *J Nucl Med.* 2018;59:1423–1429.
5. Lindner T, Loktev A, Altmann A, et al. Development of quinoline based theranostic ligands for the targeting of fibroblast activation protein. *J Nucl Med.* April 6, 2018 [Epub ahead of print].
6. Giesel F, Kratochwil C, Lindner T, et al. ^{68}Ga-FAPI PET/CT: biodistribution and preliminary dosimetry estimate of 2 DOTA-containing FAP-targeting agents in patients with various cancers. *J Nucl Med.* 2019;60:386–392.
7. Loktev A, Lindner T, Burger EM, et al. Development of novel FAP-targeted radiotracers with improved tumor retention. *J Nucl Med.* March 8, 2019 [Epub ahead of print].
8. Parghane RV, Basu S. Dual-time point ^{18}F-FDG-PET and PET/CT for differentiating benign from malignant musculoskeletal lesions: opportunities and limitations. *Semin Nucl Med.* 2017;47:373–391.
9. Tagliabue L, Del Sole A. Appropriate use of positron emission tomography with [^{18}F]fluorodeoxyglucose for staging of oncology patients. *Eur J Intern Med.* 2014; 25:6–11.
10. Jiang C, Chen Y, Zhu Y, Xu Y. Systematic review and meta-analysis of the accuracy of ^{18}F-FDG PET/CT for detection of regional lymph node metastasis in esophageal squamous cell carcinoma. *J Thorac Dis.* 2018;10:6066–6076.
11. Caresia Aroztegui AP, García Vicente AM, Alvarez Ruiz S, et al. ^{18}F-FDG PET/CT in breast cancer: evidence-based recommendations in initial staging. *Tumour Biol.* 2017;39:1010428317728285.
12. Paudyal B, Oriuchi N, Paudyal P, et al. Clinicopathological presentation of varying ^{18}F-FDG uptake and expression of glucose transporter 1 and hexokinase II in cases of hepatocellular carcinoma and cholangiocellular carcinoma. *Ann Nucl Med.* 2008;22:83–86.
13. Flechsig P, Mehndiratta A, Haberkorn U, Kratochwil C, Giesel FL. PET/MRI and PET/CT in lung lesions and thoracic malignancies. *Semin Nucl Med.* 2015; 45:268–281.
14. Kauhanen SP, Komar G, Seppänen MP, et al. A prospective diagnostic accuracy study of ^{18}F-fluorodeoxyglucose positron emission tomography/computed tomography, multidetector row computed tomography, and magnetic resonance imaging in primary diagnosis and staging of pancreatic cancer. *Ann Surg.* 2009; 250:957–963.
15. Strobel O, Büchler MW. Pancreatic cancer: FDG-PET is not useful in early pancreatic cancer diagnosis. *Nat Rev Gastroenterol Hepatol.* 2013;10:203–205.
16. Marzola MC, Chondrogiannis S, Rubello D. Fludeoxyglucose F 18 PET/CT assessment of ovarian cancer. *PET Clin.* 2018;13:179–202.
17. Kitajima K, Murakami K, Sakamoto S, Kaji Y, Sugimura K. Present and future of FDG-PET/CT in ovarian cancer. *Ann Nucl Med.* 2011;25:155–164.
18. Bertagna F, Nicolai P, Maroldi R, et al. Diagnostic role of ^{18}F-FDG-PET or PET/CT in salivary gland tumors: a systematic review. *Rev Esp Med Nucl Imagen Mol.* 2015;34:295–302.
19. Zafereo ME. Evaluation and staging of squamous cell carcinoma of the oral cavity and oropharynx: limitations despite technological breakthroughs. *Otolaryngol Clin North Am.* 2013;46:599–613.
20. Plaxton NA, Brandon DC, Corey AS, et al. Characteristics and limitations of FDG PET/CT for imaging of squamous cell carcinoma of the head and neck: a comprehensive review of anatomy, metastatic pathways, and image findings. *AJR.* 2015;205:W519–W531.
21. Lai V, Khong PL. Updates on MR imaging and ^{18}F-FDG PET/CT imaging in nasopharyngeal carcinoma. *Oral Oncol.* 2014;50:539–548.
22. Amodru V, Guerin C, Delcourt S, et al. Quantitative ^{18}F-DOPA PET/CT in pheochromocytoma: the relationship between tumor secretion and its biochemical phenotype. *Eur J Nucl Med Mol Imaging.* 2018;45:278–282.
23. Barrio M, Czernin J, Fanti S, et al. The impact of somatostatin receptor-directed PET/CT on the management of patients with neuroendocrine tumor: a systematic review and meta-analysis. *J Nucl Med.* 2017;58:756–761.
24. Hekman MCH, Rijpkema M, Aarntzen EH, et al. Positron emission tomography/computed tomography with ^{89}Zr-girentuximab can aid in diagnostic dilemmas of clear cell renal cell carcinoma suspicion. *Eur Urol.* 2018;74:257–260.
25. Antwi K, Fani M, Heye T, et al. Comparison of glucagon-like peptide-1 receptor (GLP-1R) PET/CT, SPECT/CT and 3T MRI for the localisation of occult insulinomas: evaluation of diagnostic accuracy in a prospective crossover imaging study. *Eur J Nucl Med Mol Imaging.* 2018;45:2318–2327.
26. Welt S, Divgi CR, Scott AM, et al. Antibody targeting in metastatic colon cancer: a phase I study of monoclonal antibody F19 against a cell-surface protein of reactive tumor stromal fibroblasts. *J Clin Oncol.* 1994;12:1193–1203.
27. Davidson B, Goldberg I, Kopolovic J. Inflammatory response in cervical intraepithelial neoplasia and squamous cell carcinoma of the uterine cervix. *Pathol Res Pract.* 1997;193:491–495.
28. Pandit-Taskar N, O'Donoghue JA, Beylergil V, et al. ^{89}Zr-huJ591 immuno-PET imaging in patients with advanced metastatic prostate cancer. *Eur J Nucl Med Mol Imaging.* 2014;41:2093–2105.
29. Afshar-Oromieh A, Hetzheim H, Kübler W, et al. Radiation dosimetry of ^{68}Ga-PSMA-11 (HBED-CC) and preliminary evaluation of optimal imaging timing. *Eur J Nucl Med Mol Imaging.* 2016;43:1611–1620.

JOURNAL OF NUCLEAR MEDICINE TECHNOLOGY
BEST PAPERS

▶ EDITORS' CHOICE AWARD — FOR 1st PLACE ARTICLE IN 2019

is presented to

Jena-Lee McKee, Mary Beth Farrell, Kathy Hunt, Vivian Loveless, and Charity Brannen

West Tennessee Healthcare, Dyersburg Hospital, Dyersburg, Tennessee

for

Efficiency of Radiolabeling Eggs Before and After Microwave Cooking for Gastric Emptying Scintigraphy Studies

J. Nucl. Med. Technol. 2019;47:144–148

▶ EDITORS' CHOICE AWARD — FOR 2nd PLACE ARTICLE IN 2019

is presented to

Audrey B. Davis, Melanie H. Pietryka, and Susan Passalaqua

Banner M.D. Anderson Cancer Center, Gilbert, Arizona

for

Technical Aspects and Administration Methods of ^{177}Lu-DOTATATE for Nuclear Medicine Technologists

J. Nucl. Med. Technol. 2019;47:288–291

▶ EDITORS' CHOICE AWARD — FOR 3rd PLACE ARTICLE IN 2019

is presented to

Sarah Frye, Ross Frye, Barbara Sterkel, Razi Muzaffar, and Medhat M. Osman

Clinical Health Sciences, St. Louis University, St. Louis, Missouri

for

The Need for Increased Awareness About Potential Quality Control Problems in Aging γ-Cameras

J. Nucl. Med. Technol. 2019;47:223–226

JOURNAL OF NUCLEAR MEDICINE TECHNOLOGY
BEST PAPERS

▶ EDITORS' CHOICE AWARD — FOR BEST CONTINUING EDUCATION ARTICLE IN 2019

is presented to

Geoffrey M. Currie

Faculty of Science, Charles Sturt University, Wagga Wagga, Australia, and Regis University, Boston, Massachusetts

for

Pharmacology, Part 5: CT and MRI Contrast Media

J. Nucl. Med. Technol. 2019;47:189–202

▶ EDITORS' CHOICE AWARD — FOR BEST EDUCATORS' FORUM ARTICLE IN 2019

is presented to

Cybil J. Nielsen, Sarah S. Brosmer, Patrick J. Byrne, and S. Gregory Jennings

Indiana University School of Medicine, Indianapolis, Indiana

for

An Evaluation of Qualities of Nuclear Medicine Technology Programs and Graduates Leading to Employability

J. Nucl. Med. Technol. 2019;47:29–34

2020 FREESTANDING (PRE-MEETING) SNMMI AWARD-WINNING ABSTRACTS

Arthur Weis Award in Radiation Dosimetry and Safety

Publication No.: 430
Track: Physics, Instrumentation and Data Sciences – Image Generation
Presenter: Harry Marquis
Abstract Title: SPECT/CT-based Dosimetry in PRRT: Using Theranostics to Minimise the Impact of the Partial Volume Effect
Authors/Institutions:
Harry Marquis, MMedPhys[1], Daniel Deidda, PhD[2], Ashley Gillman, PhD[3], Yaser Gholami, PhD[4], Kathy P. Willowson, PhD[5], Kris F. Thielemans, PhD[6], Dale L. Bailey, PhD[5].

[1]School of Physics, University of Sydney, Sydney, Australia, [2]National Physical Laboratory, Teddington, United Kingdom, [3]Australian e-Health Research Centre, CSIRO, Brisbane, Australia, [4]Sydney Vital Translational Cancer Research Centre, Sydney, Australia, [5]Department of Nuclear Medicine, Royal North Shore Hospital, Sydney, Australia, [6]University College London, London, United Kingdom.

Berson-Yalow Award

Publication No.: 237
Track: Molecular Targeting Probes
Presenter: Reinier Hernandez, PhD
Abstract Title: GD2/B7-H3 bispecific antibodies for next-generation neuroblastoma treatment
Authors/Institutions: Reinier Hernandez, PhD[1], Amy Erbe[1], Daniel Gerhardt[2], Jennifer Dennin[2], Christopher Massey[1], Todd E. Barnhart, PhD[1], Jonathan Ward Engle[3], Bonnie Hammer[2], Paul Sondel[1].

[1]University of Wisconsin-Madison, Madison, WI, USA, [2]Invenra, Inc., Madison, WI, USA, [3]University of Wisconsin - Madison, Madison, WI, USA.

Correlative Imaging Council/Walter Wolf Award

Publication No.: 1682
Track: Oncology: Clinical Therapy and Diagnosis -> Clinical Diagnosis ->Other Solid Tumors
Presenter: Abhishek JHA, MBBS
Abstract Title: Superiority of ^{68}Ga-DOTATATE PET/CT compared to ^{18}F-FDG PET/CT and MRI of the spine in the detection of spinal bone metastases in metastatic pheochromocytoma and/or paraganglioma
Authors/Institutions: Abhishek Jha, MBBS[1], Mayank Patel, MD[1], Babak Saboury, MD MPH[2], Corina Millo, MD[3], Alexander Ling, MD[4], Ritu Shah, MD[4], Clara C. Chen, MD[2], Leah Meuter, BS[1], Sara Talvacchio[1], Marianne Knue, CNP[1], Frank I. Lin, MD[5], Geraldine O'Sullivan Coyne[6], Alice Chen[6], Naris Nilubol[7], Peter Herscovitch, MD, FACP, FRCPC[3], David Taieb, MD, PhD[8], Ali Cahid Civelek, MD[9], Jorge A. Carrasquillo, MD[10], Karel Pacak, MD, PhD, DSc, FACE[1].

[1]Section on Medical Neuroendocrinology, Eunice Kennedy Shriver National Institute of Child Health and Human Development, National Institutes of Health, Bethesda, MD, USA, [2]Nuclear Medicine Division, Radiology and Imaging Sciences, Warren Grant Magnuson Clinical Center, National Institutes of Health, Bethesda, MD, USA, [3]Positron Emission Tomography Department, Warren Grant Magnuson Clinical Center, National Institutes of Health, Bethesda, MD, USA, [4]Radiology and Imaging Sciences, Warren Grant Magnuson Clinical Center, National Institutes of Health, Bethesda, MD, USA, [5]Molecular Imaging Program, National Cancer Institute, National Institutes of Health, Bethesda, MD, USA, [6]Division of Cancer Treatment and Diagnosis, National Cancer Institute, National Institutes of Health, Bethesda, MD, USA, [7]Surgical Oncology Program, Center for Cancer Research, National Cancer Institute, Betehsda, MD, USA, [8]La Timone Hospital, Marseille, France, [9]Nuclear Medicine, Radiology and Radiological Science, Johns Hopkins Medicine, Baltimore, MD, USA, [10]Molecular Imaging and Therapy Service, Memorial Sloan Kettering Cancer Center, New York, NY, USA

Pediatrics Imaging Council Majd-Gilday Yong Investigator Award

Publication No.: 161
Track: General Clinical Specialties -> Pediatrics
Presenter: Thomas Ng, MD
Abstract Title: Assessment of nonstandard cheese-based meals as viable alternatives to the standard adult meal for pediatric gastric emptying scintigraphy
Authors/Institutions: Thomas Ng, MD, PhD[1], Niharika Putta[2], Neha Kwatra, MD[3], Laura A. Drubach, MD[1], Frederic H. Fahey, DSc[4], Samuel Nurko, MD MPH[5], Alejandro Flores, MD[5], Stephan Voss, MD, PhD[6].

[1]Joint Program in Nuclear Medicine, Brigham and Womens Hospital, Brookline, MA, USA, [2]Brandeis University, Brookline, MA, USA, [3]Boston Children'S Hospital, Boston, MA, USA, [4]Boston Children's Hospital, Boston, MA, USA, [5]Boston Children's Hospital, Brookline, MA, USA, [6]Children's Hospital- Boston, Boston, MA, USA.

SATELLITE SYMPOSIUMS

SNMMI is pleased to offer Industry Satellite Symposiums during the Annual Meeting. These one-hour sessions provide a forum for our industry partners to directly address the nuclear medicine and molecular imaging community. SNMMI does not endorse any products or services referenced in these symposiums. No CE is offered for these sessions.

The Role of LUTATHERA® (lutetium Lu 177 dotatate) in Patients With Progressive GEP-NETs

Sunday, July 12 ▸ 1:30-2:30 pm ET

Sponsored by Advanced Accelerator Applications

Dr. Eric Liu, MD, FACS (Rocky Mountain Cancer Centers, Denver, Colorado)

Estrogen Receptor PET/CT Imaging with a Novel Biomarker: Underlying Biology, Biochemistry and Clinical Application

Sunday, July 12 ▸ 1:30-2:30 pm ET

Sponsored by Siemens Healthineers

David Mankoff, MD, PhD, Gerd Muehllehner Professor of Radiology, Perelman School of Medicine, University of Pennsylvania, Philadelphia

PSMA Imaging: Current Status and Prospects

Monday, July 13 ▸ 1:30-2:30 pm ET

Sponsored by Telix Pharmaceuticals

Alton O. Sartor MD, Piltz Professor of Cancer Research, Departments of Medicine Hematology/Medical Oncology Tulane Medical Center

Jeffery Karnes, MD, Mayo Clinic Rochester, Minn.

Jeremie Calais, MD, MSc, Assistant Professor at the Ahmanson Translational Imaging Division of the Dept. of Molecular & Medical Pharmacology

Clinical Innovations: Artificial Intelligence in PET and SPECT[1]

Monday, July 13 ▸ 1:30-2:30 pm ET

Sponsored by Siemens Healthineers

[1]syngo.via VB50 is pending 510(k) clearance and is not yet commercially available in the United States. Its future availability cannot be guaranteed.

Critical considerations in managing patients with gastroenteropancreatic neuroendocrine tumors (GEP-NETs)

Tuesday, July 14 ▸ 1:30-2:30 pm ET

Sponsored by Advanced Accelerator Applications

Dr Munir Ghesani, MD [Mount Sinai Hospital, New York]; Dr Erin E. Grady, MD [Emory University Hospital, Atlanta, Georgia]

Development & Application of Novel PET Tracer for AMPA Receptors

Tuesday, July 14 ▸ 1:30-2:30 pm ET

Sponsored by Eisai

Takuya Takahashi, MD, PhD; Professor, Department of Physiology; Yokohama City University Graduate School of Medicine, Japan

VIRTUAL EXHIBIT HALL

Visit customized virtual booths from top suppliers and learn more about their products/services through videos and downloadable presentations. Plus, connect through one-on-one meetings with exhibit personnel while visiting their booth.

EXHIBITING COMPANIES INCLUDE:

ABX-CRO advanced pharmaceutical services

ACIC - PBL

Actinium Pharmaceuticals

Advanced Accelerator Applications, a Novartis Company

Alzheimer's Association

American Board of Nuclear Medicine (ABNM)

American College of Nuclear Medicine (ACNM)

American College of Radiology (ACR)

American Society of Nuclear Cardiology (ASNC)

AnazaoHealth Corporation

Applied Nanotech, Inc.

Applied Radiology

ARRT, The American Registry of Radiologic Technologists

Asia Oceania Federation of Nuclear Medicine and Biology (AOFNMB)

Astellas Pharma US

Bayer Oncology

Bayer - Radiology

Biodex Medical Systems, Inc.

Blue Earth Diagnostics,Inc.

Bracco Diagnostics

Bruker BioSpin

Canon Medical Systems USA, Inc.

Capintec, Inc. (part of Mirion Technologies)

Cardinal Health

Comecer

Curium

Cyclomedical International, Inc.

Digirad Corporation

DMS Health

DOTmed HealthCare Business News

ec^2 Software Solutions

The Education and Research Foundation for Nuclear Medicine and Molecular Imaging (ERF)

European Association of Nuclear Medicine (EANM)

GE Healthcare

Go2 Foundation for Lung Cancer

Hermes Medical Solutions, Inc.

Huayi Isotopes Company

IBA S.A.

Ionetix Corporation

Intersocietal Accreditation Commission (IAC)

ITM Isotopen Technologien München AG

Jubilant Radiopharma

Lantheus Medical Imaging, Inc.

As of July 1, 2020

VIRTUAL EXHIBIT HALL

Visit customized virtual booths from top suppliers and learn more about their products/services through videos and downloadable presentations. Plus, connect through one-on-one meetings with exhibit personnel while visiting their booth.

EXHIBITING COMPANIES INCLUDE:

Life Molecular Imaging

Lilly

Lucerno Dynamics, LLC

MarShield Radiation Protection Products

MedImage, Inc.

Mediso Medical Imaging Systems Ltd.

MiE America

MILabs

MIM Software Inc.

MOLECUBES NV

Molecular Targeting Technologies, Inc.

MR SOLUTIONS

NorCal CarciNET Community

Northstar Medical Radioisotopes, LLC

Nuclear Medicine Technology Certification Board (NMTCB)

NUCMEDCOR

Oncidium Foundation

PETNET Solutions

Philips

PMB ALCEN

PMOD Technologies LLC

Progenics Pharmaceuticals

Progenics Pharmaceuticals - Medical Affairs

QDOSE

RadioMedix

RI-TE Radiation Imaging Technologies, Lda

SAINT-GOBAIN CRYSTALS

Scoperta Life Sciences

SHINE Medical Technologies, LLC

Siemens Healthineers

Sirona Complete Care

SOFIE

South West Exposures

Spectrum Dynamics Medical, Inc.

Sun Radiopharma (Pharmalucence)

Sylvia Fedoruk Canadian Centre for Nuclear Innovation

Telix Pharmaceuticals

Tema Sinergie

ThyCa: Thyroid Cancer Survivors' Association, Inc.

Triskem International

TTG Imaging Solutions

United Imaging

Universal Medical Resources, Inc.

US DOE Isotope Program

Versant Medical Physics and Radiation Safety

World Federation of Nuclear Medicine and Biology (WFNMB)

World Molecular Imaging Society (WMIS)

As of July 1, 2020

NETWORKING EVENTS

Special Advance Screening of “Radioactive”

Organized by the Women in Nuclear Medicine Committee (WINM)
Sponsored by Bracco Diagnostics
Saturday, July 11 ▸ beginning at 8:15 pm ET

Join your fellow attendees for this unique movie viewing party on Saturday evening! We invite you to watch and participate in a live group chat w/ friends and colleagues during a special Amazon advance screening of “Radioactive,” exclusively for Annual Meeting attendees!

“Radioactive” tells the story of Marie Curie and Pierre Curie, and the reverberation of their discoveries throughout the 20th century.

Knowledge Bowl

Tuesday, July 14 ▸ 8:30-9:30 pm ET

The SNMMI Early Career Professionals Committee (EPC) is excited to sponsor the first Virtual Knowledge Bowl! This event provides an opportunity for residents and early career professionals to network with each other in a competition of the mind! Attendees will be shown difficult general nuclear medicine and PET tracer cases, examine basic science questions and interpret important correlative imaging findings. All of this in a fun, interactive virtual platform.

NETWORKING EVENTS

Molecular Hub

Molecular Hub

Take a break from the CE sessions and join your colleagues at the Virtual Molecular Hub! Each day will feature a new topic and leaders within the field.

We invite you to begin your SNMMI Virtual Meeting experience on **Saturday, July 11 at 1:30 pm ET** . Umar Mahmood, MD, PhD, SNMMI Scientific Program Committee Chair and the SPC Cabinet will provide first time attendees with the highlights of the SNMMI meeting. The SPC will share their tips and tricks to ensuring a great meeting experience.

On **Sunday, July 12 at 9:00 am ET** join the **Council and Center Leadership** as they provide brief overviews of their activities and important information on how to get involved and connect with other individuals in your area of expertise.

Finally, on **Tuesday, July 14 at 9:00 am ET**, residents and early career professionals are invited to the join the **Early Career Professionals Committee**. ECP leaders will provide information on existing resources for early career professionals and give attendees a sneak peak of what is coming this year!

Virtual Hot Trot 5K Run/Walk

Organized by the SNMMI-TS PDEF

The Hot Trot 5K is back this year, in a virtual way. Proceeds will benefit the SNMMI-TS Professional Development and Education Fund, supporting the advancement of molecular and nuclear medicine technologists. All registered runners will receive an official race shirt and medal. Sign up by July 14.

NETWORKING EVENTS

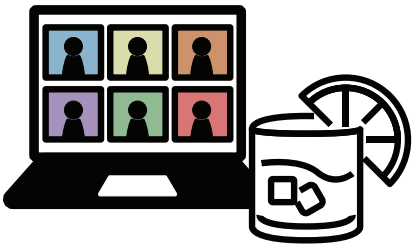

Drink and Think

Join your colleagues and friends for an informal virtual networking event. Drink and Think is where a virtual happy hour meets an exchange of scientific knowledge and discussion. The Virtual Meeting will feature two day of opportunities to participate in Drink and Think meet-ups which will include topics hosted by SNMMI Councils and Centers. We encourage you to grab a late evening snack, a drink, and be ready to discuss some of the most exciting topics in the field. A list of the schedule topics are included below:

Sunday, July 12 ▸ 8:30-9:30 pm ET pm ET

- Phased Re-opening Plans for Pediatric Nuclear Radiology Departments – *Sponsored by the Pediatric Imaging Council*
- New PET Radiopharmaceuticals: Practical Tips? – *Sponsored by the PET Center of Excellence*
- Artificial Intelligence in Nuclear Medicine – *Sponsored by the Physics, Instrumentation and Data Sciences Council*
- Prostate Imaging with PSMA PET and How it Plays into Other Imaging Modalities – *Sponsored by the Correlative Imaging Council*
- Expert Eyes on Details - Deep Cerebellar Nuclei in Neurodegenerative Imaging by Kuhl-Lassen Award Winner, Dr Nicolas Bohnen — *Sponsored by the Brain Imaging Council*
- How Toxic Environments Affect Productivity — *Sponsored by the CMIIT*

Monday, June 13 ▸ 8:15-9:15 pm ET

- Total Body PET – *Sponsored by the Physics, Instrumentation and Data Sciences Council*
- Targeted Radionuclide Therapy for Non- thyroid Pediatric Malignancies: What's Here and What's on the Horizon? – *Sponsored by the Pediatric Imaging Council*
- Nuclear Medicine and COVID-19 – *Sponsored by the General Clinical Nuclear Medicine Council*
- 21CFR2Beers...Regulatory Considerations for the Radiopharmaceutical Sciences in 2020 – *Sponsored by the Radiopharmaceutical Sciences Council*
- Nuclear Medicine Practice Optimization – Opportunity for Physician Extenders – *Sponsored by the Advanced Associate Council*
- Resident Training and Recruitment in the Time of Covid – *Sponsored by the Academic Council*
- What are You Most Excited About with the Future of Nuclear Medicine Therapies? – *Sponsored by the Therapy Center of Excellence*

NETWORKING EVENTS

SNMMI-TS President's Townhall & Reception

Saturday, July 11, 2020 ▸ 7:15 pm ET

Honoring: Mark Crosthwaite, CNMT, FSNMMI-TS — SNMMI-TS President

Attend this informal one-hour virtual town hall and reception on Saturday evening, honoring outgoing SNMMI-TS President Mark Crosthwaite, The event will feature brief remarks from Mr. Crosthwaite, the chance for you to your share your favorite stories, and more! Plus, don't miss The Thallium Stallions, who will premiere their new song "19th Coronavirus Breakdown" at the start of the reception – sponsored by Sirona Complete Care.

SNMMI President's Townhall & Reception

Monday, July 13, 2020 ▸ 7:15 pm ET

Honoring: Vasken Dilsizian, MD — SNMMI President

Attend this informal one-hour virtual town hall and reception on Monday evening, honoring outgoing SNMMI President Vasken Dilsizian, MD. The event will feature brief remarks from Dr. Dilsizian, an opportunity for your to share your favorite stories, and even some special guest surprises! We look forward to you joining the celebration.

SPONSORED BY

BRACCO
LIFE FROM INSIDE

HERMES MEDICAL SOLUTIONS

Lantheus Medical Imaging

Lilly

Thank you to our Virtual Edition Sponsors:

▶ TITLE SPONSOR

Advanced Accelerator Applications
A Novartis Company

▶ GOLD SPONSORS

Eisai

ERF
The Education and Research Foundation for Nuclear Medicine and Molecular Imaging

MILabs
Making Molecular Imaging Clear

Progenics Pharmaceuticals®
Find Fight and Follow®

SIEMENS Healthineers

▶ SILVER SPONSORS

BRACCO
LIFE FROM INSIDE

Canon
CANON MEDICAL

CURIUM™
LIFE FORWARD

HERMES MEDICAL SOLUTIONS

Lantheus
Medical Imaging

Lilly

MIM SOFTWARE

RadioMedix
INNOVATING THERANOSTICS

SPECTRUM DYNAMICS MEDICAL

TTg
Imaging Solutions

UNITED IMAGING

▶ BRONZE SPONSORS

ABX-CRO

Actinium Pharmaceuticals, Inc.

astellas

BAYER

BIODEX

BLUE EARTH DIAGNOSTICS
A Bracco Company

CAPINTEC, INC.
Part of Mirion Technologies

CardinalHealth
Essential to care™

iba

itm
PASSION FOR PRECISION

JUBILANT RADIOPHARMA

Mediso

NorthStar
MEDICAL RADIOISOTOPES, LLC

PHILIPS

▶ SATELLITE SYMPOSIUM

Advanced Accelerator Applications
A Novartis Company

Eisai

GE

SIEMENS Healthineers

TELIX PHARMACEUTICALS

Become a Sponsor

Contact Catherine Lamb at clamb@snmmi.org or Sharon Gleason at sgleason@snmmi.org today.

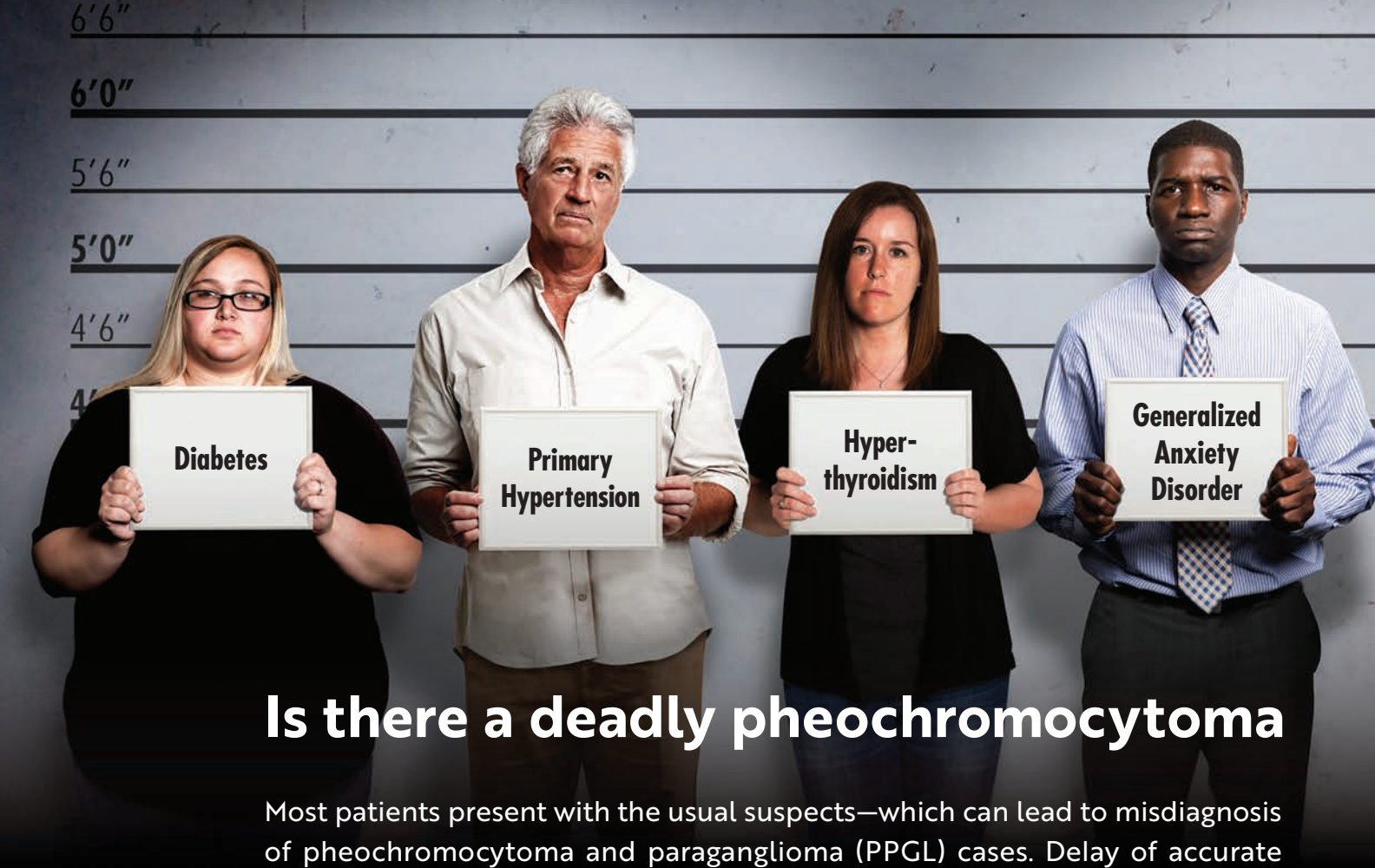

Is there a deadly pheochromocytoma

Most patients present with the usual suspects—which can lead to misdiagnosis of pheochromocytoma and paraganglioma (PPGL) cases. Delay of accurate diagnosis averages three years. During that time, patients suffer serious symptom burden, and the life-threatening disease can grow.

Patients need your help making PPGL a prime suspect.

Indication

AZEDRA® (iobenguane I 131) is indicated for the treatment of adult and pediatric patients 12 years and older with iobenguane scan positive, unresectable, locally advanced or metastatic pheochromocytoma or paraganglioma who require systemic anticancer therapy.

Important Safety Information

Warnings and Precautions:

- **Risk from radiation exposure:** AZEDRA contributes to a patient's overall long-term radiation exposure. Long-term cumulative radiation exposure is associated with an increased risk for cancer. These risks of radiation associated with the use of AZEDRA are greater in pediatric patients than in adults. Minimize radiation exposure to patients, medical personnel, and household contacts during and after treatment with AZEDRA consistent with institutional good radiation safety practices and patient management procedures.
- **Myelosuppression:** Severe and prolonged myelosuppression occurred during treatment with AZEDRA. Among the 88 patients who received a therapeutic dose of AZEDRA, 33% experienced Grade 4 thrombocytopenia, 16% experienced Grade 4 neutropenia, and 7% experienced Grade 4 anemia. Five percent of patients experienced febrile neutropenia. Monitor blood cell counts weekly for up to 12 weeks or until levels return to baseline or the normal range. Withhold and dose reduce AZEDRA as recommended in the prescribing information based on severity of the cytopenia.
- **Secondary myelodysplastic syndrome, leukemia, and other malignancies:** Myelodysplastic syndrome (MDS) and acute leukemias were reported in 6.8% of the 88 patients who received a therapeutic dose of AZEDRA. The time to development of MDS or acute leukemia ranged from 12 months to 7 years. Two of the 88 patients developed a non-hematological malignancy.
- **Hypothyroidism:** Hypothyroidism was reported in 3.4% of the 88 patients who received a therapeutic dose of AZEDRA. Initiate thyroid-blocking medications starting at least 1 day before and continuing for 10 days after each AZEDRA dose to reduce the risk of hypothyroidism or thyroid neoplasia. Evaluate for clinical evidence of hypothyroidism and measure thyroid-stimulating hormone (TSH) levels prior to initiating AZEDRA and annually thereafter.
- **Elevations in blood pressure:** Eleven percent of the 88 patients who received a therapeutic dose of AZEDRA experienced a worsening of pre-existing hypertension defined as an increase in systolic blood pressure to ≥160 mmHg with an increase of 20 mmHg or an increase in diastolic blood pressure to ≥100 mmHg with an increase of 10 mmHg. All changes in blood pressure occurred within the first 24 hours post infusion. Monitor blood pressure frequently during the first 24 hours after each therapeutic dose of AZEDRA.
- **Renal toxicity:** Of the 88 patients who received a therapeutic dose of AZEDRA, 7% developed renal failure or acute kidney injury and 22% demonstrated a clinically significant decrease in glomerular filtration rate (GFR) measured at 6 or 12 months. Monitor renal function during and after treatment with AZEDRA. Patients with baseline renal impairment may be at greater risk of toxicity; perform more frequent assessments of renal function in patients with mild or moderate impairment. AZEDRA has not been studied in patients with severe renal impairment.
- **Pneumonitis:** Fatal pneumonitis occurred 9 weeks after a single dose in one patient in the expanded access program. Monitor patients for signs and symptoms of pneumonitis and treat appropriately.
- **Embryo-fetal toxicity:** Based on its mechanism of action, AZEDRA can cause fetal harm. Verify pregnancy status in females of reproductive potential prior to initiating AZEDRA. Advise females and males of

lurking in your lineup?

When you spot it, you can treat it.

AZEDRA is the first and only FDA-approved treatment for patients 12 years and older diagnosed with iobenguane scan positive, unresectable, locally advanced or metastatic pheochromocytoma or paraganglioma who require systemic anticancer therapy. **Call 1-844-AZEDRA1 to learn more.**

- reproductive potential of the potential risk to a fetus and to use effective contraception during treatment with AZEDRA and for 7 months after the final dose. Advise males with female partners of reproductive potential to use effective contraception during treatment and for 4 months after the final dose.
- **Risk of infertility:** Radiation exposure associated with AZEDRA may cause infertility in males and females. Radiation absorbed by testes and ovaries from the recommended cumulative dose of AZEDRA is within the range where temporary or permanent infertility can be expected following external beam radiotherapy.

Adverse Reactions:
The most common severe (Grade 3–4) adverse reactions observed in AZEDRA clinical trials (≥10%) were lymphopenia (78%), neutropenia (59%), thrombocytopenia (50%), fatigue (26%), anemia (24%), increased international normalized ratio (18%), nausea (16%), dizziness (13%), hypertension (11%), and vomiting (10%). Twelve percent of patients discontinued treatment due to adverse reactions (thrombocytopenia, anemia, lymphopenia, nausea and vomiting, multiple hematologic adverse reactions).

Drug Interactions:
Based on the mechanism of action of iobenguane, drugs that reduce catecholamine uptake or that deplete catecholamine stores may interfere with iobenguane uptake into cells and therefore interfere with dosimetry calculations or the efficacy of AZEDRA. These drugs were not permitted in clinical trials that assessed the safety and efficacy of AZEDRA. Discontinue the drugs listed in the prescribing information for at least 5 half-lives before administration of either the dosimetry dose or a therapeutic dose of AZEDRA. Do not administer these drugs until at least 7 days after each AZEDRA dose.

AZEDRA®
iobenguane I 131 injection for intravenous use

For important risk and use information about AZEDRA, please see Brief Summary of Prescribing Information on adjacent pages.

To report suspected adverse reactions, contact Progenics Pharmaceuticals, Inc. at 844-668-3950 or FDA at 1-800-FDA-1088 or www.fda.gov/medwatch.

References: **1.** Young WF. Endocrine Hypertension. In: Melmed S, et al. *Williams Textbook of Endocrinology.* 13th ed. Philadelphia, PA: Elsevier; 2016. **2.** Handler J. *J Clin Hypertens.* 2007;9:293-296. **3.** Agarwal V, Kant G, Hans N, et al. *Int J Cardiol.* 2011;153:241-248. **4.** Martucci VL, Pacak K. *Curr Probl Cancer.* 2014;38(1):7-41. **5.** Lefebvre M, Foulkes WD. *Curr Oncol.* 2014;32(1):e8-e17. **6.** Kantorovich V, Eisenhofer G, Pacak K. *Ann NY Acad Sci.* 2009;1148:462-468. **7.** AZEDRA® prescribing information. New York, NY: Progenics Pharmaceuticals, Inc.; 08 2018.

AZEDRA® is a registered trademark of Progenics Pharmaceuticals, Inc. All trademarks, registered or otherwise, are the property of their respective owner (s).

© 2019 Progenics Pharmaceuticals, Inc. PM-US-AZ-0260

Progenics Pharmaceuticals®
Find Fight and Follow®

AZEDRA®

iobenguane I 131 injection for intravenous use

The following is a Brief Summary; refer to the full Prescribing Information for complete information at www.AZEDRA.com

INDICATIONS AND USAGE

AZEDRA is indicated for the treatment of adult and pediatric patients 12 years and older with iobenguane scan positive, unresectable, locally advanced or metastatic pheochromocytoma or paraganglioma who require systemic anticancer therapy.

DOSAGE AND ADMINISTRATION

Important Safety Information

AZEDRA is a radiopharmaceutical. Handle with appropriate safety measures to minimize radiation exposure. Use waterproof gloves and effective radiation shielding when handling AZEDRA. Radiopharmaceuticals, including AZEDRA, should be used by or under the control of physicians who are qualified by specific training and experience in the safe use and handling of radiopharmaceuticals, and whose experience and training have been approved by the appropriate governmental agency authorized to license the use of radiopharmaceuticals.

Verify pregnancy status in females of reproductive potential prior to initiating AZEDRA.

Recommended Dosage

Administer thyroid blockade and other pre- and concomitant medications as recommended.

Dosimetric Dose

The recommended AZEDRA dosimetric dose administered as an intravenous injection is:

- Patients weighing greater than 50 kg: 185 to 222 MBq (5 or 6 mCi)
- Patients weighing 50 kg or less: 3.7 MBq/kg (0.1 mCi/kg)

Dosimetry and Biodistribution Assessment

Following the AZEDRA dosimetric dose:

- Acquire anterior/posterior whole body gamma camera images within 1 hour of the AZEDRA dosimetric dose and prior to patient voiding (Day 0; Scan 1).
- Acquire additional images on Day 1 or 2 following patient voiding (Scan 2).
- Acquire additional images between Days 2-5 following patient voiding (Scan 3).

For each individual patient, calculate the radiation dose estimates to normal organs and tissues per unit activity [D (organ)] of administered dose using data extracted from these 3 images. Calculate in accordance with the Medical Internal Radiation Dose (MIRD) schema or related methodology. Whenever possible, use patient-specific organ masses (e.g. estimated from imaging).

Therapeutic Dosage

The recommended AZEDRA therapeutic dose is based on body weight and reduced, if necessary, based on the dosimetry data. Administer a total of 2 therapeutic doses intravenously a minimum of 90 days apart.

Weight Based Dose per Therapeutic Cycle

- Patients weighing greater than 62.5 kg: 18,500 MBq (500 mCi)
- Patients weighing 62.5 kg or less: 296 MBq/kg (8 mCi/kg)

Determine if Dose Reduction Needed Based on Critical Organ Limits

- Calculate the estimated critical organ absorbed-dose by multiplying the dosimetry-derived radiation absorbed-dose per unit activity [D (organ)] by weight based therapeutic total activity (Aw).
- If resulting estimated critical organ absorbed-dose is less than threshold absorbed-dose (T) shown in Table 1, no dose adjustment is necessary.
- If resulting estimated critical organ absorbed-dose exceeds threshold absorbed-dose (T) shown in Table 1, calculate the reduced therapeutic total activity (i.e., the cumulative activity that would be administered in 2 therapeutic cycles) using the following equation:

  Reduced Therapeutic Total Activity= Aw × [T ÷ {Aw × D (organ)}]

- Example: A 75 kg patient qualifies for a therapeutic total activity of 1000 mCi (Aw). For the kidneys, the dosimetry yields an estimated critical organ absorbed dose per unit activity of 0.027 Gy/mCi [D (kidney)]. Thus, the estimated critical organ absorbed-dose to the kidney is 27 Gy [Aw x D (organ)], which exceeds the threshold absorbed-dose for the kidneys (T) of 18 Gy (Table 1). Using the equation above the reduced therapeutic total activity to be administered to this patient is 666.7 mCi.

  1000 mCi × [18 Gy ÷ {1000 mCi × 0.027 Gy/mCi }]

Table 1: Absorbed-dose Threshold Values for Radiation Toxicity in Critical Organs

Organ	~ 1%-rate: mortality or organ failure associated with disease	Time to death or organ failure	Threshold* absorbed-dose for ~1%-rate mortality or organ failure (Gy)
Red marrow	H-ARS mortality	1-2 months	12
Lungs	Pneumonitis mortality	1-7 months	16.5
Kidneys	Renal failure	>1 year	18
Liver	Hepatomegaly, ascites: possible organ failure	0.5-3 months	31
Small intestine	GI-ARS mortality	6-9 days	40

* Threshold of ~0.5 Gy for both heart and carotid artery, derived from experience with external-beam radiotherapy and associated with fractionated exposure, has also been proposed to support an ~1% mortality rate of cardiovascular and cerebrovascular deaths in >10-15 years. Great uncertainty is associated with the value ~ 0.5 Gy cited for vascular disease (ICRP publication 118, p.300, Table 4.5), consider benefits/risks to patients.

Thyroid Blockade and Other Pre- and Concomitant Medications

Thyroid Blockade

Administer inorganic iodine starting at least 24 hours before and continuing for 10 days after each AZEDRA dose.

Hydration

Instruct patients to increase fluid intake to at least two liters a day starting at least 1 day before and continuing for 1 week after each AZEDRA dose to minimize irradiation to the bladder.

Drugs that Reduce Catecholamine Uptake or Deplete Stores

Discontinue drugs that reduce catecholamine uptake or deplete catecholamine stores for at least 5 half-lives before administration of either the dosimetry dose or a therapeutic dose of AZEDRA. Do not administer these drugs until at least 7 days after each AZEDRA dose.

Antiemetic

Administer antiemetics 30 minutes prior to administering each AZEDRA dose.

Dose Modifications for Adverse Reactions

Recommended dose modifications of AZEDRA for adverse reactions are provided in Table 2 and the recommended dose or dose reduction for the second therapeutic dose of AZEDRA for myelosuppression are provided in Table 3.

Table 2: Recommended Dose Modifications of AZEDRA for Adverse Reactions

Adverse Reaction	Dose Modification
Myelosuppression	Do not administer the first therapeutic dose for platelet counts less than 80,000/mcL or absolute neutrophil counts (ANC) less than 1,200/mcL. Do not administer the second therapeutic dose until platelets and neutrophils return to baseline or to the normal range. Reduce the second therapeutic dose for the following: • platelet count less than 25,000/mcL, ANC less than 500/mcL, or life-threatening anemia for more than 7 days • febrile neutropenia • platelet count less than 50,000/mcL with active bleeding
Pneumonitis	• Do not administer the second therapeutic dose if pneumonitis is diagnosed after the first therapeutic dose.

Table 3: Recommended Dose or Dose Reduction for Second Therapeutic Dose of AZEDRA for Myelosuppression

Patient Population	If first therapeutic dose was weight based,	If first therapeutic dose was reduced based on critical organ limits,
Patients weighing greater than 62.5 kg	Reduce the second therapeutic dose to 425 mCi	Reduce second therapeutic dose to 85% of the first dose
Patients weighing 62.5 kg or less	Reduce the second therapeutic dose to 7 mCi/kg	Reduce second therapeutic dose to 85% of the first dose

DOSAGE FORMS AND STRENGTHS

Injection: 555 MBq/mL (15 mCi/mL) as a clear, colorless to pale yellow solution in a single-dose vial.

WARNINGS AND PRECAUTIONS

Risk from Radiation Exposure

AZEDRA contributes to a patient's overall long-term radiation exposure. Long-term cumulative radiation exposure is associated with an increased risk for cancer. These risks of radiation associated with the use of AZEDRA are greater in pediatric patients than in adults.

Minimize radiation exposure to patients, medical personnel, and household contacts during and after treatment with AZEDRA consistent with institutional good radiation safety practices and patient management procedures.

Myelosuppression

Severe and prolonged myelosuppression occurred during treatment with AZEDRA. Among the 88 patients who received a therapeutic dose of AZEDRA, 33% experienced Grade 4 thrombocytopenia, 16% experienced Grade 4 neutropenia, and 7% experienced Grade 4 anemia. Five percent of patients experienced febrile neutropenia. In Study IB12B following the first therapeutic dose, patients who experienced Grade 4 neutropenia reached neutrophil nadir at a median of 36 days (27 – 55 days) and remained at nadir for a median of 12 days (8 – 22 days) until recovery to less than or equal to Grade 3. Following the second dose, patients who experienced Grade 4 neutropenia reached nadir at a median of 43 days (38 – 47 days) and remained at nadir for a median of 18.5 days (8 – 31 days) until recovery to less than or equal to Grade 3.

Monitor blood cell counts weekly for up to 12 weeks or until levels return to baseline or the normal range. Withhold and dose reduce AZEDRA as recommended based on severity of the cytopenia.

Secondary Myelodysplastic Syndrome, Leukemia and Other Malignancies

Myelodysplastic syndrome (MDS) or acute leukemias were reported in 6.8% of the 88 patients who received a therapeutic dose of AZEDRA. The time to development of MDS or acute leukemia ranged from 12 months to 7 years.

Two of the 88 patients developed a non-hematological malignancy. One patient developed colon cancer at 18 months and one patient developed lung adenocarcinoma at 27 months following the first therapeutic dose.

Hypothyroidism

Hypothyroidism was reported in 3.4% of the 88 patients who received a therapeutic dose of AZEDRA. The time to worsening of hypothyroidism was 4 months in one patient, and the time to development of hypothyroidism was less than one month in one patient and 18 months in one patient. Initiate thyroid-blocking medications starting at least 1 day before and continuing for 10 days after each AZEDRA dose to reduce the risk of hypothyroidism or thyroid neoplasia. Evaluate for clinical evidence of hypothyroidism and measure thyroid-stimulating hormone (TSH) levels prior to initiating AZEDRA and annually thereafter.

Elevations in Blood Pressure

Eleven percent of the 88 patients who received a therapeutic dose of AZEDRA experienced a worsening of pre-existing hypertension defined as an increase in systolic blood pressure to ≥160 mmHg with an increase of 20 mmHg or an increase in diastolic blood pressure to ≥ 100 mmHg with an increase of 10 mmHg. All changes in blood pressure occurred within the first 24 hours post infusion. Monitor blood pressure frequently during the first 24 hours after each therapeutic dose of AZEDRA.

Renal Toxicity

Of the 88 patients who received a therapeutic dose of AZEDRA, 7% developed renal failure or acute kidney injury and 22% demonstrated a clinically significant decrease in glomerular filtration rate (GFR) measured at 6 or 12 months. Monitor renal function during and after treatment with AZEDRA. Patients with baseline renal impairment may be at greater risk of toxicity; perform more frequent assessments of renal function in patients with mild or moderate impairment. AZEDRA has not been studied in patients with severe renal impairment (creatinine clearance <30 mL/min).

Pneumonitis

Fatal pneumonitis occurred 9 weeks after a single dose in one patient in the expanded access program for Study IB12B (n=11). Pneumonitis was not diagnosed among the 88 patients enrolled in Study IB12 or IB12B. Monitor patients for signs and symptoms of pneumonitis and treat appropriately.

Embryo-Fetal Toxicity

Based on its mechanism of action, AZEDRA can cause fetal harm. There are no available data on the use of AZEDRA in pregnant women. No animal studies using iobenguane I 131 have been conducted to evaluate its effect on female reproduction and embryo-fetal development; however, all radiopharmaceuticals, including AZEDRA, have the potential to cause fetal harm.

Verify pregnancy status in females of reproductive potential prior to initiating AZEDRA.

Advise females and males of reproductive potential of the potential risk to a fetus. Advise females of reproductive potential to use effective contraception during treatment with AZEDRA and for 7 months after the final dose. Advise males with female partners of reproductive potential to use effective contraception during treatment and for 4 months after the final dose.

Risk of Infertility

Radiation exposure associated with AZEDRA may cause infertility in males and females. The recommended cumulative dose of 37 GBq of AZEDRA results in a radiation absorbed dose to the testes and ovaries within the range where temporary or permanent infertility can be expected following external beam radiotherapy.

ADVERSE REACTIONS

The following serious adverse reactions are described elsewhere in the labeling:

- Myelosuppression
- Secondary Myelodysplastic Syndrome, Leukemia and Other Malignancies
- Hypothyroidism
- Elevations in Blood Pressure
- Renal Toxicity
- Pneumonitis

Clinical Trials Experience

Because clinical trials are conducted under widely varying conditions, adverse reaction rates observed in the clinical trials of a drug cannot be directly compared to rates in the clinical trials of another drug and may not reflect the rates observed in practice.

The data in Warnings and Precautions reflect exposure to AZEDRA in 88 patients with iobenguane-scan positive recurrent or unresectable, locally advanced or metastatic pheochromocytoma or paraganglioma (PPGL) who received a therapeutic dose of AZEDRA in one of two clinical studies (IB12 or IB12B). The Warnings and Precautions also include data from 11 patients enrolled in an expanded access program for Study IB12B.

The safety data below was evaluated in two studies in patients with recurrent or unresectable, locally advanced or metastatic PPGL. Study

IB12 was an open-label, multi-center, single-arm dose-finding study in adult patients with malignant or recurrent PPGL. The study consisted of a 12-month efficacy phase with a 1 year follow-up. Twenty-one patients received a dosimetric dose (~5 mCi), followed by one therapeutic dose (~500 mCi) of AZEDRA. Study IB12B was an open-label, multi-center, single-arm study in 68 adult and pediatric patients age 12 years and older with recurrent or unresectable, locally advanced or metastatic PPGL.

Patients with evidence of liver dysfunction (aspartate aminotransferase or alanine aminotransferase ≥ 2.5 times the upper limit of normal or total bilirubin > 1.5 times the upper limit of normal), a history of liver disease (including hepatitis and chronic alcohol abuse), or severe renal impairment (creatinine clearance < 30 mL/min) were excluded. Patients who had received external beam radiation to > 25% of bone marrow, received whole body radiotherapy, or who had received any systemic radiotherapy resulting in myelosuppression within 3 months of study entry, were also excluded. The safety data described below are based on pooled safety data from studies IB12 and IB12B. A total of 88 patients received at least one therapeutic dose of AZEDRA and 50 patients received two therapeutic doses (one patient received treatment in both studies).

Adverse reactions from studies IB12 and IB12B are presented in Table 4. The most common severe (Grade 3-4) adverse reactions were lymphopenia (78%), neutropenia (59%), thrombocytopenia (50%), fatigue (26%), anemia (24%), increased international normalized ratio (18%), nausea (16%), dizziness (13%), hypertension (11%), and vomiting (10%). Twelve percent of patients discontinued treatment due to adverse reactions (thrombocytopenia, anemia, lymphopenia, nausea and vomiting, multiple hematologic adverse reactions).

Table 4: Adverse Reactions Occurring in ≥10% of Patients with PPGL Receiving Therapeutic Dose of AZEDRA in Studies IB12B and IB12

Adverse Reaction	All Grades[a], (%)	Grades[a] 3 - 4, (%)
Hematologic[b]		
Lymphopenia	96	78
Anemia	93	24
Thrombocytopenia	91	50
Neutropenia	84	59
Gastrointestinal		
Nausea	78	16
Vomiting[c]	58	10
Dry mouth	48	2
Sialadenitis[d]	39	1
Diarrhea	25	3
Abdominal pain[e]	23	6
Constipation	19	7
Oropharyngeal pain	14	0
Dyspepsia	10	0
General		
Fatigue[f]	71	26
Pyrexia	14	2
Injection site pain	10	0
Hyperhidrosis	10	0
Alopecia	10	0
Infections		
Upper respiratory tract infection[g]	16	2
Urinary tract infection	11	1
Investigations[b]		
International normalized ratio increased[h]	85	18
Increased blood alkaline phosphatase	53	5
Increased aspartate aminotransferase	50	2
Increased alanine aminotransferase	43	2
Metabolism and nutrition		
Decreased appetite	30	5
Dehydration	16	4
Decreased weight	16	1
Musculoskeletal and connective tissue disorders		
Back pain	17	2
Pain in extremity	15	0
Nervous system		
Dizziness[i]	34	13
Headache	32	6
Dysgeusia[j]	24	1
Respiratory, thoracic, and mediastinal disorders		
Cough	18	0
Dyspnea	18	7
Vascular		
Hypotension	24	4
Hypertension[k]	20	11
Tachycardia	10	3

[a] NCI CTCAE version 3.0.
[b] Based on laboratory data.
[c] Includes vomiting and retching.
[d] Includes sialoadenitis, salivary gland pain, and salivary gland enlargement.
[e] Includes abdominal pain, abdominal pain upper, and abdominal pain lower.
[f] Incudes fatigue, asthenia.
[g] Includes upper respiratory tract infection, sinusitis, rhinorrhea, upper-airway cough syndrome, nasopharyngitis.
[h] Only assessed in Study IB12B (N=68).
[i] Includes dizziness and dizziness postural.
[j] Includes dysgeusia, hypogeusia and ageusia.
[k] Includes blood pressure increased and hypertension.

The following clinically significant adverse reactions were observed in < 10% of patients treated with AZEDRA:

Cardiac: palpitations (9%), syncope and presyncope (8%)

Endocrine: decreased TSH (5%), hypothyroidism (3%)

Gastrointestinal: dysphagia (7%), abdominal distension (6%), gastroesophageal reflux disease (6%), stomatitis (3%)

General: insomnia (9%), chills (8%), chest pain (6%)

Infections: candida infection (6%)

Investigations: prolonged prothrombin time (9%)

Musculoskeletal and connective tissue: arthralgia (8%), neck pain (8%), pain in jaw (7%), muscle spasms (6%)

Renal and urinary disorders: proteinuria (9%), renal failure (7%),

Respiratory: epistaxis (9%), nasal congestion (7%), pulmonary embolism (3%)

Skin and subcutaneous tissue: dry skin (8%), rash (8%), petechiae (7%)

Vascular: orthostatic hypotension (9%).

DRUG INTERACTIONS

Drugs that Reduce Catecholamine Uptake or Deplete Stores

Based on the mechanism of action of iobenguane, drugs that reduce catecholamine uptake or that deplete catecholamine stores may interfere with iobenguane uptake into cells and therefore interfere with dosimetry calculations or the efficacy of AZEDRA. These drugs were not permitted in clinical trials that assessed the safety and efficacy of AZEDRA. Discontinue drugs that reduce catecholamine uptake or deplete catecholamine stores, such as those listed below, for at least 5 half-lives before administration of either the dosimetry dose or a therapeutic dose of AZEDRA. Do not administer these drugs until at least 7 days after each AZEDRA dose.

- CNS stimulants or amphetamines (e.g. cocaine, methylphenidate, dextroamphetamine)
- Norepinephrine and dopamine reuptake inhibitors (e.g. phenteramine)
- Norepinephrine and serotonin reuptake inhibitors (e.g. tramadol)
- Monoamine oxidase inhibitors (e.g. phenelzine and linezolid)
- Central monoamine depleting drugs (e.g. reserpine)
- Non-select beta adrenergic blocking drugs (e.g. labetalol)
- Alpha agonists or alpha/beta agonists (e.g. pseudoephedrine, phenylephrine, ephedrine, phenylpropanolamine, naphazoline)
- Tricyclic antidepressants or norepinephrine reuptake inhibitors (e.g. amitriptyline, buproprion, duloxetine, mirtazapine, venlafaxine)
- Botanicals that may inhibit reuptake of norephinephrine, serotonin or dopamine (e.g. ephedra, ma huang, St John's Wort, or yohimbine)

USE IN SPECIFIC POPULATIONS

Pregnancy

Risk Summary

Based on its mechanism of action, AZEDRA can cause fetal harm. There are no available data on AZEDRA use in pregnant women. No animal studies using iobenguane I 131 have been conducted to evaluate its effect on female reproduction and embryo-fetal development; however, all radiopharmaceuticals, including AZEDRA, have the potential to cause fetal harm. Advise pregnant women of the risk to a fetus.

In the U.S. general population, the estimated background risk of major birth defects and miscarriage in clinically recognized pregnancies is 2 to 4% and 15 to 20%, respectively.

Lactation

Risk Summary

There are no data on the presence of iobenguane I 131 in human milk or its effects on the breastfed infant or milk production. No lactation studies in animals were conducted. Because of the potential risk for serious adverse reactions in breastfed infants, advise women not to breastfeed during treatment with AZEDRA and for 80 days after the final dose.

Females and Males of Reproductive Potential

Pregnancy Testing

Verify pregnancy status in females of reproductive potential prior to initiating AZEDRA.

Contraception

AZEDRA can cause fetal harm when administered to a pregnant woman.

Females
Advise women of reproductive potential to use effective contraception during treatment with AZEDRA and for 7 months following the final dose of AZEDRA.

Males
Based on its mechanism of action, advise males with female partners of reproductive potential to use effective contraception during treatment with AZEDRA and for 4 months following the final dose of AZEDRA.

Infertility

The recommended cumulative dose of 37 GBq of AZEDRA results in a radiation absorbed dose to the testes and ovaries within the range where temporary or permanent infertility can be expected following external beam radiotherapy.

Pediatric Use

The safety and effectiveness of AZEDRA have been established in patients 12 years and older with unresectable and iobenguane scan positive, locally advanced or metastatic, pheochromocytoma and paraganglioma (PPGL) which require systemic anticancer therapy. Use of AZEDRA for this indication is supported by evidence from an adequate and well-controlled study in adults and pediatric patients 12 years and older.

The risks of radiation associated with AZEDRA is greater in pediatric patients than that in adult patients due to greater absorbed radiation doses and longer life expectancy. Ensure the therapeutic benefit of AZEDRA outweighs these greater risks prior to administration in pediatric patients.

The safety and effectiveness of AZEDRA have not been established in pediatric patients younger than 12 years old with unresectable and iobenguane scan positive, locally advanced or metastatic PPGL which require systemic anticancer therapy.

Geriatric Use

Of the patients enrolled in all clinical studies of AZEDRA, 17% were 65 years or older and 1% were 75 years or older. Clinical studies of AZEDRA did not include sufficient numbers of subjects aged 65 and over to determine whether they respond differently from younger subjects.

Renal Impairment

The radiation dose to patients with renal impairment may be increased due to the delayed elimination of the drug. Adjust the therapeutic dose based on radiation exposure estimates from the dosimetry assessment. The safety of AZEDRA in patients with severe renal impairment (CLcr < 30 mL/min) or end-stage renal disease has not been studied.

NONCLINICAL TOXICOLOGY

Carcinogenesis, Mutagenesis, Impairment of Fertility

Carcinogenicity studies with iobenguane I 131 have not been conducted; however, radiation is a carcinogen and a mutagen. No animal studies were conducted to determine the effects of iobenguane I 131 on fertility.

PATIENT COUNSELING INFORMATION

Hydration

Advise patients to drink at least 2 liters of liquid a day before and for one week following each dose of AZEDRA to minimize irradiation of the bladder.

Radiation Risks

Advise patients to minimize radiation exposure to household contacts consistent with institutional good radiation safety practices and patient management procedures.

Myelosuppression

Advise patients to contact their health care provider for any signs or symptoms of neutropenia, thrombocytopenia, or anemia.

Secondary Myelodysplastic Syndrome, Leukemia and Other Malignancies

Advise patients of the potential for secondary cancers, including myelodysplastic syndrome, acute leukemia, and other malignancies.

Hypothyroidism

Advise patients to take thyroid-blocking agents as prescribed. Advise patients of the need for life-long monitoring for hypothyroidism.

Elevations in Blood Pressure

Advise patients to contact their health care provider for signs or symptoms that may occur following tumor-hormone catecholamines release and possible risk of increased blood pressure during or 24 hours following each therapeutic AZEDRA dose.

Pneumonitis

Advise patients to contact their health care provider for signs or symptoms of pneumonitis.

Drug Interactions

Advise patients that some medicines interact with AZEDRA and to contact their health care provider before starting any over the counter medicines or herbal or dietary supplements.

Embryo-Fetal Toxicity

Advise pregnant women and males and females of reproductive potential of the potential risk to a fetus. Advise females to inform their health care provider of a known or suspected pregnancy.

Advise females of reproductive potential to use effective contraception during treatment with AZEDRA and for 7 months after the final dose.

Advise male patients with female partners of reproductive potential to use effective contraception during treatment with AZEDRA and for 4 months after the final dose.

Lactation

Advise females not to breastfeed during treatment with AZEDRA and for 80 days after the final dose.

Infertility

Advise females and males patients that AZEDRA may impair fertility.

Manufactured for:
Progenics Pharmaceuticals, Inc.
One World Trade Center, 47th floor, Suite J
New York, NY 10007
AZEDRA® is a registered trademark of Progenics Pharmaceuticals, Inc.

The Hot Trot 5K is back this year, in a virtual way. Proceeds will benefit the SNMMI-TS Professional Development and Education Fund, supporting the advancement of molecular and nuclear medicine technologists. All registered runners will receive an official race shirt and medal. Sign up by July 14.

Learn more at:
www.snmmi.org/HotTrot5k

Professional Development and Education Fund
PDEF
Give. Learn. Lead.

SNMMI 2020 Annual Meeting

SNMMI Society of Nuclear Medicine and Molecular Imaging
Technologist Section
50 YEARS • 1970-2020

THE BRANDS YOU KNOW

THE QUALITY YOU TRUST

TechneLite®
Technetium Tc 99m Generator

NEUROLITE®
KIT FOR THE PREPARATION OF TECHNETIUM Tc99m BICISATE FOR INJECTION

Xenon
Xe 133 Gas

QUADRAMET®
(SAMARIUM SM 153 LEXIDRONAM INJECTION)

Cardiolite®
Kit for the Preparation of
Technetium Tc99m Sestamibi for Injection

Gallium
Gallium Citrate
Ga 67 Injection

Thallium
Thallous Chloride
Tl 201 Injection

To order, please contact your
Lantheus Nuclear Products Sales Representative
or call Customer Service 1-800-299-3431
Monday – Friday 7:30 AM – 6:00 PM EST

Lantheus
Medical Imaging®

For full Prescribing Information on each of the Lantheus products, please visit www.lantheus.com

TechneLite, NEUROLITE, Cardiolite, QUADRAMET, Lantheus Medical Imaging and the corporate logo are registered trademarks of Lantheus Medical Imaging, Inc. ©2020 Lantheus Medical Imaging, Inc. All rights reserved. NUC 220 June 2020